UG-DFM-2/97
FTUV/97-18
IFIC/97-18

Many Body approach to the inclusive (e, e') reaction from the quasielastic to the Δ excitation region

A. Gil[1], J. Nieves[2] and E. Oset[1]

[1] *Departamento de Física Teórica and IFIC, Centro Mixto Universidad de Valencia - CSIC, 46100 Burjassot (Valencia) Spain.*

[2] *Departamento de Física Moderna, Universidad de Granada, 18071 Granada, Spain.*

Abstract

We have performed a many body calculation of the inclusive (e, e') cross section which runs over the three traditional regions at intermediate energies: the quasielastic peak, the dip region and the delta region. The longitudinal and transverse response functions in the quasielastic peak have also been evaluated. Traditional effects like polarization, meson exchange currents, final state interaction and delta renormalization in the nuclear medium have been included. Meson exchange currents are generated from a model of pion electroproduction on the nucleon which reproduces accurately the experimental data.

The inclusive cross section accounts for $1N, 2N, 3N$ mechanisms of virtual photon absorption and one pion production. Meson exchange currents associated to the $(\gamma^*, 2\pi)$ reaction are also accounted for.

We obtain good results for the (e, e') cross sections in the whole energy range and for different nuclei. The response functions are also in good agreement with the latest experimental analysis. On the other hand, the method provides the separation of the contribution to the inclusive cross section from different physical channels which is a necessary input to evaluate cross sections like $(e, e'N)$, $(e, e'NN)$, $(e, e'\pi)$ etc.

1 Introduction

Inclusive electron scattering, particularly around the quasielastic peak is probably one of the problems that has attracted more attention in nuclear physics. One of the reasons for the proliferation of theoretical work was the persistent difficulty of simple

pictures based on the shell model of the nucleus, or the Fermi gas approach, to reproduce simultaneously the longitudinal and the transverse response functions around the quasielastic peak. Particularly, the longitudinal response appeared systematically to be much larger than experiment [1, 2, 3].

Even more worrisome was the fact that the integrated strength of the experimental longitudinal response function showed large discrepancies with the expected result according to the Coulomb sum rule [4]. At large values of the momentum transfer q this integral should be the charge of the nucleus and there was some apparent missing strength.

Those experimental results have been generally accepted, even when some other experimental results seemed to challenge them. Indeed the results of the experiment of [5] in ^{238}U did not show the expected suppression of the longitudinal response. More recently an experiment at Bates on ^{40}Ca [6] showed a longitudinal response larger than in ref. [1] with only 20% reduction over the simple shell model expectations.

The growing experimental discrepancies stimulated the thorough and thoughtful work of [7]. In this work the author analysed the world set of data and made further improvements in the analysis, coming with new results for the response functions which show a smaller reduction of the longitudinal response than previously assumed. At the heart of the issue was the fact that, in a modified Rosenbluth plot in terms of the variable ϵ (which runs from 0 to 1), the Saclay data [1, 2, 3] concentrated their points in the region of $\epsilon < 0.5$ which induces large errors in the slope of the straight line which correlates the points of the plot. Those results, complemented by others at SLAC and Bates, which fill up the region of $\epsilon \sim 1$, lead to a more accurate determination of the slope and thus the longitudinal response. The problems with the Coulomb sum rule are then automatically solved [7] to the relief of all [8].

As usually happens, some theoretical calculations were "successful" in explaining the abnormal reductions of the longitudinal response, through the use of small effective masses, swelling of nucleons, abnormal nucleon form factors, correlations, etc. But in the benefit of the theoretical community it should be said that whenever this happened, the agreement with the transverse response was spoiled, although excuses and good wishes beyond the ideas used for the longitudinal response were invoked as possible solutions. Hence, a convincing simultaneous explanation of both the longitudinal and transverse response functions was never obtained.

The interesting thing is that the existence of a "problem" induced so much work that practically all resources of nuclear physics and many body theory have been used in this topic and a lot of things have been learned. In the present work we shall benefit from all this previous work and by using a selfcontained many body formalism we will incorporate all these effects which convincingly proved to be relevant in previous works. We also incorporate some new ingredients which come out naturally within our many body expansion and furthermore we include Delta–hole (Δh) excitations, additional to the particle–hole (ph) excitations, which allows us to simultaneously study the quasielastic peak, the Δ peak and the "dip" region between the two peaks in the inclusive (e, e') cross section.

2 Brief review of different approaches and introduction to our approach.

The amount of ideas which have been studied in connection with the inclusive (e, e') scattering is quite large. We shall discuss them briefly:

2.1 Modification of the nucleon form factor (swelling of the nucleon)

These ideas were soon invoked and explored within different frameworks [9, 10]. They appear naturally in some microscopic models of the nucleon form factor when the intermediate baryon propagators are replaced by those in the nuclear medium. This is the case, for instance in ref. [11], where the underlying elementary model is the Nambu-Jona-Lasinio model of the nucleon. Obviously there are many other medium effects not taken into account in these schemes, as we shall see. Furthermore, although in a different language and in terms of a few relevant physical magnitudes, such medium modifications appear in a systematic many body expansion, where they can be classified as vertex corrections.

2.2 Relativistic effects

Theories using relativistic scalar and vector potentials like in the Walecka model [12] have been popular. The scalar and vector potentials are about one order of magnitude larger than the ordinary non relativistic potential which is roughly the sum of the two. This cancellation is missed in many applications of these relativistic potentials leading to unrealistic predictions. The appealing thing of the relativistic approach is the small effective mass, $M_N^* \simeq M_N/2$ of the nucleon and the fact that the nucleon response for ph excitations is roughly proportional to M_N^*. This reduces the longitudinal response but also the transverse one.

A clarifying view of these problems is exposed in [13] where the necessity to go beyond the relativistic mean field approach is shown in order to avoid the pathological predictions tied to the small effective masses, like in the computation of the nuclear response functions or the large relativistic enhancements that drive magnetic moments outside their Schmidt lines. In [13] a relativistic RPA calculation is used. Similar conclusions are found in [14], stating that "selfconsistent calculations" show cancellations between large relativistic effects on the single nucleon current and on the many nucleon wave functions. In [15] it is also shown, by solving numerically the Dirac equation with the relativistic potential, that the genuine relativistic effects in the enhancement of the axial charge amount to 20-30%, while perturbative calculations give as much as 70-80% enhancement [16, 17].

Even when improved with some selfconsistent steps, relativistic calculations still rely on the concept of the effective mass [13, 18, 19], which is only an approximation to the richer content of the nucleon self-energy. The nucleon self-energy is a function of the energy and momentum, as independent variables, and leads to important dynam-

ical properties of the nucleus [20] not contained in static pictures like the mean field theories. One of the consequences is that the nucleon effective mass is a strongly dependent function of the energy, with a peak around the Fermi surface [20]. Furthermore, as shown in [21], RPA correlations tied to the pionic degrees of freedom are essential in order to provide the energy dependence of the nucleon self-energy and hence the dynamical properties of the nucleus. Actually it is quite interesting to see that recent sophisticated calculations in light nuclei using path integral Monte Carlo methods [22] find that "pion degrees of freedom in both nuclear interaction and currents play a crucial role in reproducing the experimental data".

From this discussion it looks clear that improvements along the relativistic line for the present problem should include "selfconsistency" in the sense of ref. [14], in order to exploit the large cancellations between the scalar and vector potentials.

2.3 Pionic effects

As mentioned above [22], the pionic degrees of freedom play an important role in quasielastic electron scattering. This has also been emphasized in [23] where meson exchange currents driven by pion exchange are evaluated, putting special emphasis in fulfilling the continuity equation and preserving gauge invariance in the many body system. This imposition has as a consequence some changes in the results with respect to former works along similar lines [24, 25, 26]

In ref. [27] similar ideas, but using the formalism of path integrals is followed. RPA correlations are automatically generated in that scheme leading to some quenching of the longitudinal response from a reduction in the isoscalar channel.

Pions are also explicitly used in approaches which include meson exchange currents, as we shall see below. They are usually taken static, as in [23, 27], meaning that the energy carried by the pion is neglected. While this is a fair approximation for the exchange currents at energies below pion production threshold, at higher energies the need to work will the full pion propagator becomes apparent. This is particularly true if one wishes to account for real pion production in the same many body scheme, as we shall do.

In the resonance region primary pion production accounts for the largest part of the response function (although some of the pions are absorbed in their way out of the nucleus and show up in $2N$ or $3N$ emission channels). Hence, the explicit treatment of pionic degrees of freedom allowing pions to be produced, both as virtual as well as real states, becomes a necessity in this region. Our scheme puts a special emphasis on pions. In fact it follows a different path to other schemes, beginning with real pion production and ensuring that a proper hand on the $(e, e'\pi)$ reaction is held. Then exchange currents and further corrections in the many body system are generated from the model for the $eN \to e'N\pi$ reaction.

2.4 Meson exchange currents

A large fraction of work has been devoted to the role played by meson exchange currents (MEC) in this reaction [23, 24, 25, 26, 28, 29, 30]. The standard seagull, pion

in flight and Δ terms are included mediated by pions. The indirect effect of short range correlations in these terms is, however, neglected in those works. The work of [31] incorporates terms in the scheme which account for virtual photon absorption on correlated pairs, hence accounting for ground state correlations. Although the same concepts are shared in the previous approaches, differences in the input and the way to implement them lead to different results.

Our approach differs from the quoted works although conceptually it is quite similar. First we realize that the two body currents appear in (e, e') as corrections to the main one body contribution. This is because virtual photons can be absorbed by one nucleon. This is opposite to the case of real photons which require at least two nucleons to be absorbed (we are thinking in terms of infinite nuclear matter). Thus it is clear that the laboratory to test the effect of two nucleon currents is real photons not virtual ones. This is the reason why prior to the present work we devoted energies to the problem of real photon absorption [32]. Second, in order to minimize sources of uncertainties, the MEC were generated from the model $\gamma N \to \pi N$ by allowing the pion to be produced in a virtual state and be absorbed by a second nucleon. After this is done, long range correlations from polarization phenomena, as well as short range correlations, are taken into account. The model for the $\gamma N \to \pi N$ reactions was tested against experimental data and was found to be good. This gives one some confidence in the strength that one generates for the MEC. The reliability of the method gets extra support from recent measurements of two body photon absorption [33, 34, 35] where the agreement with the (γ, np) emission channels is rather good. Some discrepancies remain in the (γ, pp) channel, but this channel has an experimental cross section nearly one order of magnitude smaller than the (γ, np) one, thus for the purpose of the total (γ, NN) emission or the two body MEC in (e, e') such discrepancies will not play an important role.

In view of the success in the real photon case, we adopt here the same scheme and follow the same steps simply substituting the real photon by the virtual one. This means that we begin with a model for the $eN \to e'N\pi$ reaction and construct the MEC from it following identical steps to those of ref. [32]. For this reason we begin in next section by showing our model for the $eN \to e'N\pi$ reaction and contrasting it with the experimental results.

2.5 RPA correlations

Several works have emphasized the role played by RPA correlations allowing for a ph excitation which propagates in the nuclear medium mediated by some residual ph interaction [13, 27, 36, 37]. These works share the feature that a reduction is produced in the longitudinal channel. We shall also incorporate these long range correlations or polarization effects. In addition we shall also include Δh excitations, as a source for polarization which will be relevant in the transverse channel as shown in [38].

2.6 Final state interaction (FSI)

This is another topic which has received some attention and a thorough work devoted to this issue can be seen in [39]. It is clear that once a ph excitation is produced by the virtual photon, the outgoing nucleon can collide many times, thus inducing the emission of other nucleons. A distorted wave approximation with an optical (complex) nucleon nucleus potential would remove all these events. However, if we want to evaluate the inclusive (e, e') cross section these events should be kept and one must sum over all open final state channels [40, 39]. This is done explicitly in [39] and the result of it is a certain quenching of the quasielastic peak of the simple ph excitation calculation and a spreading of the strength to the sides of it, or widening of the peak. The integrated strength over energies is not much affected though.

The use of correlated wave functions, evaluated from realistic NN forces and incorporating the effects of the nucleon force in the nucleon pairs has also been advocated in connection with the effects from final state interaction [41]. If one incorporates two particle–two hole ($2p2h$) components in the final excited states one gets the spreading of the peaks as found in [39]. For the purpose of the response function it is like exciting ph components which have a decay width into the $2p2h$ channel. This gives rise to the quenching of the peak and spreading of the strength. Another source of these effects is the momentum dependence of the nucleon self-energy which is also accounted for in the scheme and which sometimes is taken into account approximately in terms of an effective mass (although our position on evaluations which use this variable has been already made clear). The approach of [41] using an orthogonal correlated basis with functions obtained with variational methods also incorporates RPA correlations discussed in point 5) but does not account for the MEC discussed in point 4), which rely upon the coupling of the photon to the pion or the Δ excitations.

In our many body scheme we will account for this FSI by using nucleon propagators properly dressed with a realistic self-energy in the medium, which depends explicitly on the energy and the momentum [42]. This self-energy leads to nucleon spectral functions in good agreement with other accurate more microscopic approaches like the ones in [43, 44]. The self-energy of [42] has the proper energy–momentum dependence plus an imaginary part from the coupling to the $2p2h$ components, hence it has the ingredients to account for the FSI effects discussed in [41] although using a different calculational scheme.

Nuclear spectral functions with a language closer to the one we shall follow have also been used in [45]. They include the interesting result, which we will employ here, that keeping the width of the particle states is important but one can disregard the width of the hole states.

2.7 Δ excitation

While many efforts have been devoted to the quasielastic peak very little attention has been given to the Δ region and the dip region between the quasielastic and Δ peaks. One exception is the work of [46] which looks at the effects of MEC in the dip region.

A recent work [47] presents some experimental results and a theoretical analysis of

the Δ region based on the $eN \to e'N\pi$ model of [48]. One interesting conclusion of the work is that the data have a broader energy spectrum than the theoretical one based on the properties of a free Δ width. This suggest a larger Δ width from Δ coupling to many body channels, additional to the natural decay width with effects of Fermi motion included. This is actually well known from pion physics [49, 50].

Our aim in this section is also to evaluate as accurately as possible the response function in this region, for which we shall use results for the Δ in a nuclear medium [51] which have been tested thoroughly in a variety of pionic reactions: elastic [52], quasielastic, charge exchange, absorption, etc... [53].

The discussion in this sections has served to expose relevant works done in the literature and to present our approach in connection to the ideas exposed in these works. We shall follow a microscopic many body description of the inclusive (e, e') process and will incorporate in our approach the important effects discussed in this section. We are thus aiming at an evaluation as accurate as possible at the present moment. A small sacrifice is made in order to allow one to treat microscopically in a tractable way all the effects discussed above: we use an infinite nuclear medium and obtain results for finite nuclei using the local density approximation (LDA). This was also used for the evaluation of the total cross section of real photons with nuclei with good results [32] and a mathematical derivation was made there to justify the accuracy of the approximation. A direct comparison of results with the LDA with finite nucleus results, using the same input was done in [54] for deep inelastic lepton scattering, showing that indeed the LDA is an excellent approximation to deal with volume processes (i.e no screening or absorption effects). In [55] a comparison of the results for finite nuclei with those of the Fermi gas around the quasielastic (e, e') peak is done, showing that for some average Fermi momentum, the results of the Fermi gas and those of finite nuclei are nearly identical, proposing that choice as an even better prescription than the LDA. We shall follow the LDA, already tested for real photons, and sufficiently good for our purposes.

Another feature which is novel in our approach and rather important in practical terms is the following: we shall use a method which relates the (e, e') cross section to the imaginary part of the virtual photon self-energy. This is actually not new and has been used before [13, 56]. The novelty is that by using properly Cutkosky rules one can relate the different sources of imaginary part to different channels which contribute to the inclusive (e, e') cross section. In this way, we lay the grounds to evaluate from the present input the cross sections for exclusive processes $(e, e'N)$, $(e, e'NN)$, $(e, e'\pi)\,(e, e'N\pi)$ etc., which will be the subject of a forthcoming paper [57]. The results of the present paper and those of [57] are part of a PhD thesis [58] where additional details to those given here can be found if desired.

3 The $eN \to e'N\pi$ reaction

3.1 Formalism

We shall follow the model used in ref. [32] for $\gamma N \to \pi N$ at intermediate energies generalizing it to virtual photons. In fact this model is essentially the same as used for the $eN \to eN\pi$ reaction in [48]. However, having in mind the application to nuclei we make a reduction of the relativistic amplitudes keeping terms up to $O(\frac{P}{M_N})$, with, P,M_N the nucleon momentum and mass. The neglect of the $O(\frac{P}{M_N})^2$ terms is justified numerically as we shall see in the results, so we construct this non relativistic amplitude for the $eN \to eN\pi$ process ready to be used with ordinary non relativistic nucleon wave functions.

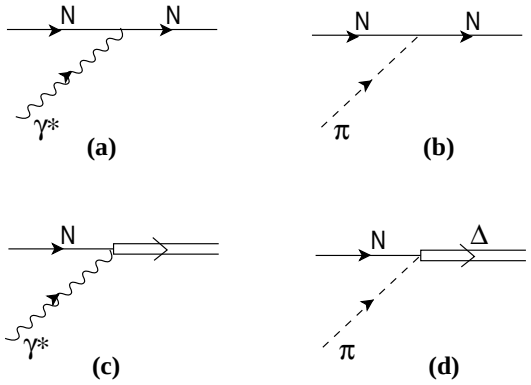

Fig.3.1 Basic couplings of the virtual photon and the pion to the nucleon and to the $N\Delta$ transition.

The basic couplings which we need are those depicted in fig.3.1 which account for the coupling of the photon and the pion to the nucleon and to the $N\Delta$ transition, plus the Kroll Ruderman term (KR), and the coupling of the photon to the pion. The Kroll Ruderman term appears as a gauge invariant term through minimal substitution when a pseudovector πNN coupling is used, as we do. The analytical expressions for these vertices are given in appendix A. For convenience, from the KR term of the appendix coming from gauge invariance, and which we call there seagull term, we construct the KR term displayed in this chapter such that it contains all the non vanishing pieces of the amplitude when $p_\pi \to 0$. We will come back to this point later on.

3.2 The amplitudes for the $eN \to eN\pi$ model

The Feynman diagrams which are considered in the model for $\gamma N \to \pi N$ of [32] or in $\gamma^* N \to \pi N$ of [48] (γ^* will stand from now on for the virtual photon) are depicted in fig. 3.2.

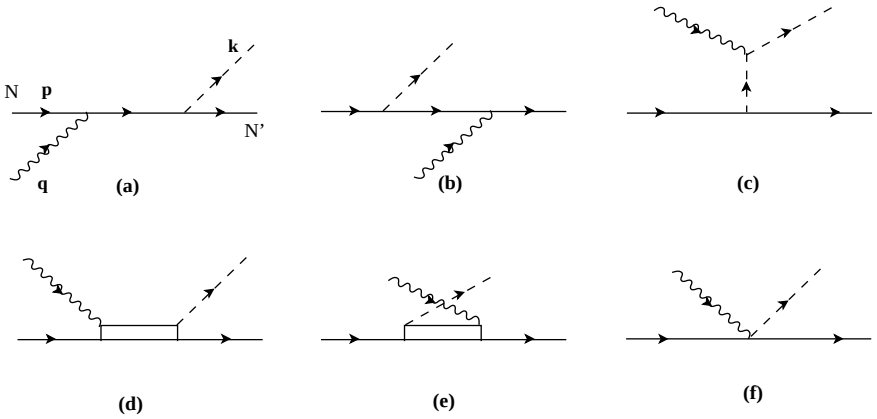

Fig.3.2 Feynman diagrams considered for the $\gamma^* N \to \pi N$ reaction.

They are the nucleon pole direct (NP) term (a), the nucleon pole crossed (NPC) term (b), the pion pole (PP) term (c), the delta pole direct (DP) term (d), delta pole crossed (DPC) term (e) and Kroll Ruderman (KR) term (f). The expressions for these amplitudes are obtained by doing the nonrelativistic reduction of the relativistic amplitudes of [48]. There is some small contribution from the negative energy intermediate nucleon states which is kept in our expressions, which as we mentioned neglect only terms of order $O(\frac{P}{M_N})^2$. The corresponding expressions are:

$$\mathcal{M}^{\mu}_{NP} = -e\frac{f_{\pi NN}}{m_\pi} B(N,N'\pi)\frac{1}{\sqrt{s}-M_N} F_\pi((q-k)^2)\times$$

$$\times \begin{pmatrix} F_1^N(q^2)\vec{\sigma}\vec{k} \\ \\ F_1^N(q^2)\vec{\sigma}\vec{k}\left[\frac{2\vec{p}+\vec{q}}{2M_N}\right] + i\frac{\vec{\sigma}\vec{k}}{2M_N}(\vec{\sigma}\times\vec{q})G_M^N(q^2) \end{pmatrix} \tag{1}$$

$$\mathcal{M}^{\mu}_{KR} = e\frac{f_{\pi NN}}{m_\pi} B(N,N'\pi) F_A(q^2) C^\mu(\pi,N') F_\pi((q-k)^2) \tag{2}$$

where

$$C^\mu(\pi^- p) = \begin{pmatrix} \frac{\vec{\sigma}\vec{q}}{2M_N} \\ \\ \left(1+\frac{q^0}{2M_N}\right)\vec{\sigma} \end{pmatrix} \quad ; \quad C^\mu(\pi^0 n) = 0$$

$$C^\mu(\pi^+ n) = \begin{pmatrix} \frac{\vec{\sigma}\vec{q}}{2M_N} \\ \\ -\left(1-\frac{q^0}{2M_N}\right)\vec{\sigma} \end{pmatrix} \quad ; \quad C^\mu(\pi^0 p) = \begin{pmatrix} \frac{\vec{\sigma}\vec{q}}{M_N} \\ \frac{q^0}{M_N}\vec{\sigma} \end{pmatrix}$$

$$\mathcal{M}^{\mu}_{PP} = -e_\pi \frac{f_{\pi NN}}{m_\pi} B(N,N'\pi)\vec{\sigma}(\vec{k}-\vec{q}) F_{\gamma\pi\pi}(q^2)\frac{(2k-q)^\mu}{(k-q)^2-m_\pi^2} F_\pi((q-k)^2) \tag{3}$$

$$\mathcal{M}^{\mu}_{NPC} = -e\frac{f_{\pi NN}}{m_\pi}B(N,N'\pi)\frac{1}{p^0-k^0-E(\vec{p}-\vec{k})}F_\pi((q-k)^2)\times$$

$$\times\begin{pmatrix} F_1^{N'}(q^2)\vec{\sigma}\vec{k} \\ F_1^{N'}(q^2)\left\{\frac{2\vec{p}+\vec{q}-2\vec{k}}{2M_N}\right\}\vec{\sigma}\vec{k}+G_M^{N'}(q^2)i\frac{(\vec{\sigma}\times\vec{q})\vec{\sigma}\vec{k}}{2M_N}\end{pmatrix} \tag{4}$$

with

$$\begin{aligned} B(n,n\pi^0) &= -1 \\ B(n,p\pi^-) &= \sqrt{2} \\ B(p,p\pi^0) &= 1 \\ B(p,n\pi^+) &= \sqrt{2} \end{aligned}$$

If we consider,

$$\begin{aligned} I(\pi^0) &= I_c(\pi^0) = 2/3 \\ I(\pi^+) &= -I_c(\pi^+) = -\sqrt{2}/3 \\ I(\pi^-) &= -I_c(\pi^-) = \sqrt{2}/3 \end{aligned}$$

we get

$$\mathcal{M}^{\mu}_{DP} = -if^*\frac{f_\gamma(q^2)}{m_\pi^2}\frac{\vec{S}\left[\vec{k}-\frac{k^0}{\sqrt{s}}\vec{p}_\Delta\right]}{\sqrt{s}-M_\Delta+i\frac{\Gamma(s)}{2}}\frac{\sqrt{s}}{M_\Delta}I(\pi)\times$$

$$\times\begin{pmatrix} \frac{\vec{p}_\Delta}{\sqrt{s}}\left(\vec{S}^\dagger\times\vec{q}\right) \\ \frac{p^0_\Delta}{\sqrt{s}}\left[\vec{S}^\dagger\times\left(\vec{q}-\frac{q^0}{p^0_\Delta}\vec{p}_\Delta\right)\right]\end{pmatrix} \tag{5}$$

$$\mathcal{M}^{\mu}_{DPC} = -if^*\frac{f_\gamma(q^2)}{m_\pi^2}\left(\frac{M_N}{M_\Delta}\right)\frac{(E_\Delta+M_\Delta)}{(p^2_\Delta-M^2_\Delta)}I_c(\pi)\times$$

$$\times\begin{pmatrix} 0 \\ (\vec{S}\times\vec{q})(\vec{S}^\dagger\vec{k}\,)-\vec{B}\end{pmatrix} \tag{6}$$

with

$$\vec{B} = \frac{1}{3}\left\{i\frac{(k^0+a)}{E_\Delta+M_\Delta}(\vec{q}^{\,2}\vec{\sigma}-(\vec{q}\vec{\sigma})\vec{q})+\frac{(k^0-a)}{2M_N}[(\vec{q}\times\vec{p}\,)-i(\vec{q}\vec{p}\,)\vec{\sigma}+i\vec{p}\,(\vec{\sigma}\vec{q})]\right\}$$

$$a = (p_\Delta k)\frac{1}{M_\Delta}$$

where $\sqrt{s}$ is the invariant energy of the system virtual photon-initial nucleon, $e(e>0)$ is the electron charge, $m_\pi = 139.5$ MeV is the pion mass, $M_\Delta = 1238$ MeV, the Δ mass [32] and the free decay width of the Δ is given by

$$\Gamma(s) = \frac{1}{6\pi}\left(\frac{f^*}{m_\pi}\right)^2 \frac{M_N}{\sqrt{s}}|\vec{k}_{cm}|^3\Theta(\sqrt{s}-M_N-m_\pi) \tag{7}$$

On the other hand, $f_{\pi NN}, f_\gamma, f^*, F_1, G_M, F_A, F_{\gamma\pi\pi}, F_\pi$, are coupling constants and form factors which we show in the appendix, as well as $\vec{S}$, the spin transition operator from spin 3/2 to 1/2.

The expressions given keep the Lorentz covariance up to terms $O(\frac{P}{m_N})^2$. The small Δ crossed term of eq.(6) holds strictly in the frame where the outgoing nucleon is at rest.

As mentioned before, in the KR term of eq.(2) we have included corrections in the zero component which come from the zero component of the NP and NCP terms when using the vertex of eq.(104) (this means from positive energy intermediate states). On the other hand the $q^0/2M_N$ terms in the spatial components of the KR term come from the intermediate negative energy components of the NP and NCP relativistic amplitudes. This trick serves us to concentrate on the KR term all the contributions which do not vanish when the pion momentum goes to zero.

3.3 Gauge invariance and form factors

Gauge invariance implies that $q_\mu\mathcal{M}^\mu = 0$ where $\mathcal{M}^\mu = \sum_i \mathcal{M}_i^\mu$. From the expressions given above we can see that the delta terms are gauge invariant by themselves. As for the rest of the amplitudes they form a block of gauge invariance terms in the absence of form factors. However, we must impose some restrictions in order to keep gauge invariance when the form factors are included. If we consider the $\gamma^* n \to p\pi^-$ amplitude we see

$$q_\mu\mathcal{M}^\mu \frac{1}{e\dfrac{f_{\pi NN}}{m_\pi}B(N,N'\pi)} =$$

$$= -\frac{1}{p^0-k^0-E(\vec{p}-\vec{k})}\left\{\left(q_0F_1^p - \frac{(2\vec{p}\,\vec{q}-2\vec{k}\vec{q}+\vec{q}^{\,2})}{2M_N}F_1^p\right)\vec{\sigma}\vec{k}\right\} \tag{8}$$

$$-\vec{\sigma}\vec{q}F_A - F_{\gamma\pi\pi}\vec{\sigma}(\vec{k}-\vec{q}) = 0$$

which together imply

$$\Rightarrow \left[F_1^p(q^2) = F_{\gamma\pi\pi}(q^2) = F_A(q^2)\right] \tag{9}$$

Gauge invariance in other isospin channels does not require extra relationships. In the Appendix we can see that $\Lambda \simeq M_A \simeq \sqrt{2}p_\pi$ and hence eq. (9) is fulfilled to a good degree of approximation. However, in order to keep strict gauge invariance we take only one form factor for all, which we choose to be F_1^p of eq.(108). We have checked that by taking any of the other form factors the changes induced in the cross sections

are much smaller than the experimental errors (see fig.3.6), so we are rather safe with any of these choices.

On the other hand, since in the pion pole term we have a form factor corresponding to the coupling πNN with a virtual pion, $F_\pi((q-k)^2)$, we have included this form factor in the amplitudes of this block (NP,NCP,PP,KR) in order to preserve gauge invariance.

3.4 Unitarity

Another refinement introduced in the model is unitarity. Watson's theorem implies that the phase of the $\pi N \to \pi N$ and $\pi N \to \gamma N$ amplitudes in each term of the partial wave decomposition must be the same. Such as our model stands, we have a Δ term which by itself satisfies the theorem if we assume the $\pi N \to \pi N$ amplitude dominated by the Δ, as it is the case. However, in the $\gamma N \to \pi N$ amplitude we have a sizeable background that in our model is real and the sum of the terms does not satisfy Watson's theorem. Although this violation of unitary does not result in important numerical changes in the cross section, we nevertheless unitarize the model as was done for real photons [32]. We follow the procedure of [59] introducing a small phase $\phi(\sqrt{s}, q^2)$ which corrects the Δ term, where $\sqrt{s}$ is the invariant energy of the virtual photon-initial nucleon system and q^2 the four–momentum squared of the virtual photon. By means of an iterative method we find $\phi(\sqrt{s}, q^2)$ such that

$$Im\left[(T_\Delta(q^2)e^{i\phi(\sqrt{s},q^2)} + T_B(q^2))^{(3/2,3/2)} e^{-i\delta_{(3/2,3/2)}(q^2)}\right] = 0 \tag{10}$$

where $T_\Delta(q^2)$ represents the Δ pole direct term amplitude, $T_B(q^2)$ is the contribution of the rest of the terms to the (3/2, 3/2) channel (see details in [32] for the projection of these terms in the (3/2, 3/2) channel) and $\delta_{(3/2,3/2)}(q^2)$ are the πN phase shifts in the 3/2,3/2 spin-isospin channel.

3.5 Cross sections for the $eN \to eN\pi$ process

We follow here the steps and nomenclature of ref. [60]. In fig.3.3 we show diagrammatically the process with the different variables which we use, k_e, k'_e, q, p, p' and k representing the momenta of the incoming electron, outgoing electron, virtual photon, initial nucleon, final nucleon and pion respectively.

The unpolarized cross section is given by [60]:

$$\frac{d^2\sigma}{d\Omega'_e dE'_e} = \frac{\alpha^2}{q^4}\frac{|\vec{k}'_e|}{|\vec{k}_e|} L_{\mu\nu}(e,e')\bar{W}^{\mu\nu}_{e.m.} \tag{11}$$

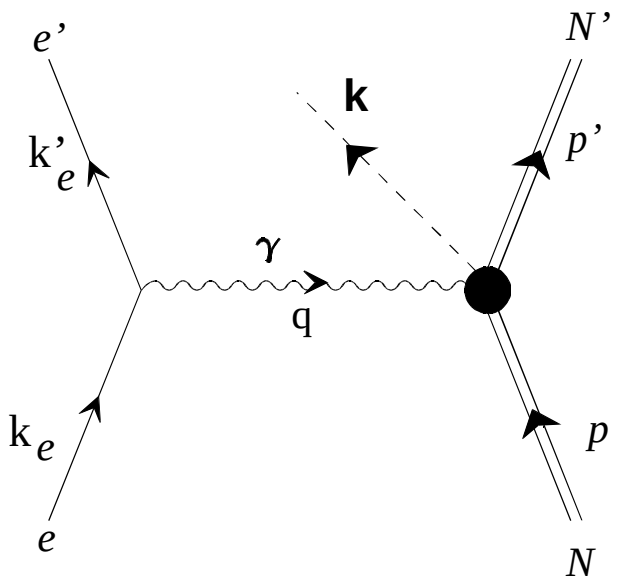

Fig.3.3 Feynman diagram for the $eN \to e'N\pi$ process.

where $\alpha = 1/137.036$ is the fine structure constant ($e^2/4\pi$) and $L_{\mu\nu}$ the leptonic tensor defined as

$$L_{\mu\nu}(e,e') = 2(k_{e\mu}' k_{e\nu} + k_{e\nu}' k_{e\mu} + \frac{q^2}{2} g_{\mu\nu}) \tag{12}$$

The hadronic tensor is given by

$$\begin{aligned} \bar{W}_{em}^{\mu\nu} = & \overline{\sum_{spin}} \int \frac{d^3p_N'}{(2\pi)^3} \frac{M_N}{E'} \int \frac{d^3k}{(2\pi)^3} \frac{1}{2E_\pi} (2\pi)^3 \times \\ & \times \delta^4(p_N' + k - p_N - q) < N'\pi|j_{em}^\mu|N >^* < N'\pi|j_{em}^\nu|N > \end{aligned} \tag{13}$$

with j_{em}^μ the $\gamma^* N$ to $N'\pi$ amplitude defined in sect. 3.2.

We can separate from there the angular dependence of the pion and get

$$\frac{d^3\sigma}{d\Omega_e' dE_e' d\Omega_\pi} = \frac{\alpha^2}{q^4} \frac{|\vec{k}_e'|}{|\vec{k}_e|} L_{\mu\nu}(e,e') W_{e.m.}^{\mu\nu}(N) \tag{14}$$

where now

$$\begin{aligned} W_{em}^{\mu\nu} = & \overline{\sum_{spin}} \int \frac{d^3p_N'}{(2\pi)^3} \frac{M_N}{E'} \int \frac{dk\, \vec{k}^2}{(2\pi)^3 2E_\pi} (2\pi)^3 \times \\ & \times \delta^4(p_N' + k - p_N - q) < N'\pi|j_{em}^\mu|N >^* < N'\pi|j_{em}^\nu|N > \end{aligned} \tag{15}$$

Now by taking $\vec{q}$ along the z direction, using gauge invariance and the explicit expressions for $L_{\mu\nu}$ we can write, following exactly the same steps as in [60, 48]

$$\frac{d^5\sigma}{d\Omega'_e dE'_e d\Omega^*_\pi} = \Gamma\left\{\frac{d\sigma_T}{d\Omega^*_\pi} + \epsilon\frac{d\sigma_L}{d\Omega^*_\pi} + \epsilon\frac{d\sigma_p}{d\Omega^*_\pi}cos2\Phi^*_\pi + \right.$$
$$\left. + \sqrt{2\epsilon(1+\epsilon)}\frac{d\sigma_I}{d\Omega^*_\pi}cos\Phi^*_\pi\right\} \tag{16}$$

where

$$\epsilon = \left[1 - 2\frac{|\vec{q}|^2}{q^2}tg^2\left(\frac{\theta_e}{2}\right)\right]^{-1}$$
$$\Gamma = \frac{\alpha}{2\pi^2}\frac{|\vec{k}'_e|}{|\vec{k}_e|}\left[-\frac{1}{q^2}\right]\frac{k_\gamma}{1-\epsilon} \tag{17}$$
$$k_\gamma = \frac{s - M_N^2}{2M_N}$$

and

$$\frac{d\sigma_T}{d\Omega^*_\pi} = \frac{e^2}{64\pi^2 k_\gamma}\frac{M_N}{\sqrt{s}}|\vec{k}_{CM}|\left[(J^{xx} + J^{yy})\right]^{CM}_{\Phi^*_\pi=0}$$
$$\frac{d\sigma_L}{d\Omega^*_\pi} = \frac{-q^2}{(q^0_{cm})^2}\frac{e^2}{32\pi^2 k_\gamma}\frac{M_N}{\sqrt{s}}|\vec{k}_{CM}|\left[J^{zz}_{CM}\right]_{\Phi^*_\pi=0}$$
$$\frac{d\sigma_p}{d\Omega^*_\pi} = \frac{e^2}{64\pi^2 k_\gamma}\frac{M_N}{\sqrt{s}}|\vec{k}_{CM}|\left[(J^{xx} - J^{yy})\right]^{CM}_{\Phi^*_\pi=0} \tag{18}$$
$$\frac{d\sigma_I}{d\Omega^*_\pi} = -\sqrt{\frac{-q^2}{(q^0_{cm})^2}}\frac{e^2}{64\pi^2 k_\gamma}\frac{M_N}{\sqrt{s}}|\vec{k}_{CM}|\left[(J^{zx} + J^{xz})\right]^{CM}_{\Phi^*_\pi=0}$$

where the variables of the electron are in the lab frame while those of the pion are in the $\gamma^* N$ CM frame. $J^{\mu\nu}$ in the former expressions is given by

$$J^{\mu\nu} = Tr(j^{\dagger\mu}_{em} j^{\nu}_{em}) \tag{19}$$

The angular variables $\theta_e, \theta^*_\pi, \Phi^*_\pi$ are depicted in fig. 3.4. The variables k_e, k'_e determine the (e, e') reaction plane and $\vec{q}$, the virtual photon momentum, determines the z direction. The $\vec{q}$ direction and the pion momentum $\vec{k}$ determine the πN reaction plane, and the angle between this plane and the (e, e') plane is the angle Φ^*_π.

The normalization of $d\sigma_i/d\Omega^*_\pi$ is chosen in such a way that in the limit of real photons $d\sigma_i/d\Omega^*_\pi$ coincides with the unpolarized cross section of $\gamma N \to \pi N$ with real photons. In this case the variable k_γ becomes the lab momentum of the real photon. The variables $\sigma_T, \sigma_L, \sigma_p, \sigma_I$ are the so called transverse, longitudinal, polarization and interference cross sections, respectively.

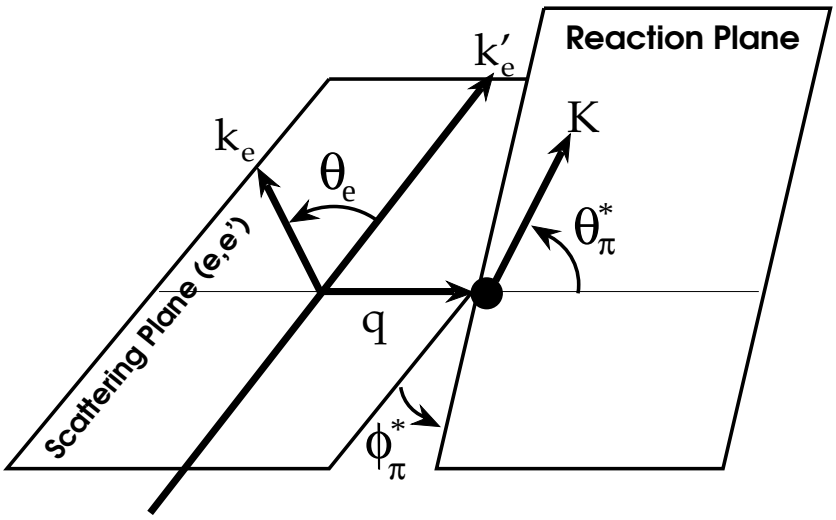

Fig.3.4 Angular variables $\theta_e, \theta^*_\pi, \Phi^*_\pi$ in the $eN \to e'N\pi$ process.

3.6 Results for $eN \to eN\pi$

In fig. 3.5 we show the $W = \sqrt{s}$ dependence of the longitudinal (lower line) and transverse (upper line) cross sections summing over the final charge of the pion and integrating over Ω^*_π. The peak position, the strength and the shape of our results are in good agreement with the data of [61]. In general terms our results are very close to those obtained in [48] with a similar good agreement with experiment as found there.

In fig. 3.6, and as an illustration of our discussion about gauge invariance in sect. 3.3, we show the differences between the results for the inclusive cross sections σ_T and σ_L, obtained: by using F_A and taking (as gauge invariance forces) $F_1^p = F_{\gamma\pi\pi} = F_A$ (dotted lines); by using $F_{\gamma\pi\pi}$ and taking $F_1^p = F_A = F_{\gamma\pi\pi}$ (dash lines); by using F_1^p and taking $F_A = F_{\gamma\pi\pi} = F_1^p$ (full lines) and, finally, by using F_A, $F_{\gamma\pi\pi}$ and F_1^p (dash-dotted lines). As one can see, the differences are negligible, relative to present experimental errors.

In fig. 3.7 we show the results for $d\sigma_I/d\Omega^*_\pi/(\sin\theta^*_\pi\sqrt{2})$ in the channel $ep \to en\pi^+$ and compare them with the experimental data of [62]. We can see that the agreement is reasonably good and so is the case for $d\sigma_P/d\Omega^*_\pi/\sin^2\theta^*_\pi$ shown in fig. 3.8, where the data are again from [62].

In fig. 3.9 we show the Φ^*_π dependence of the cross section in the channel $ep \to en\pi^+$ for three different kinematics. The data are from [62] and we see again a reasonable agreement with experiment.

Finally in fig. 3.10 we show the Φ^*_π dependence for another channel, the $ep \to ep\pi^0$, in order to show a case where the agreement with the data, in this case from ref. [63], is not as good as in general terms. Given the fact that the angle Φ^*_π will be integrated in the (e, e') reactions in nuclei, such punctual discrepancies will not matter in our study of the nuclear processes.

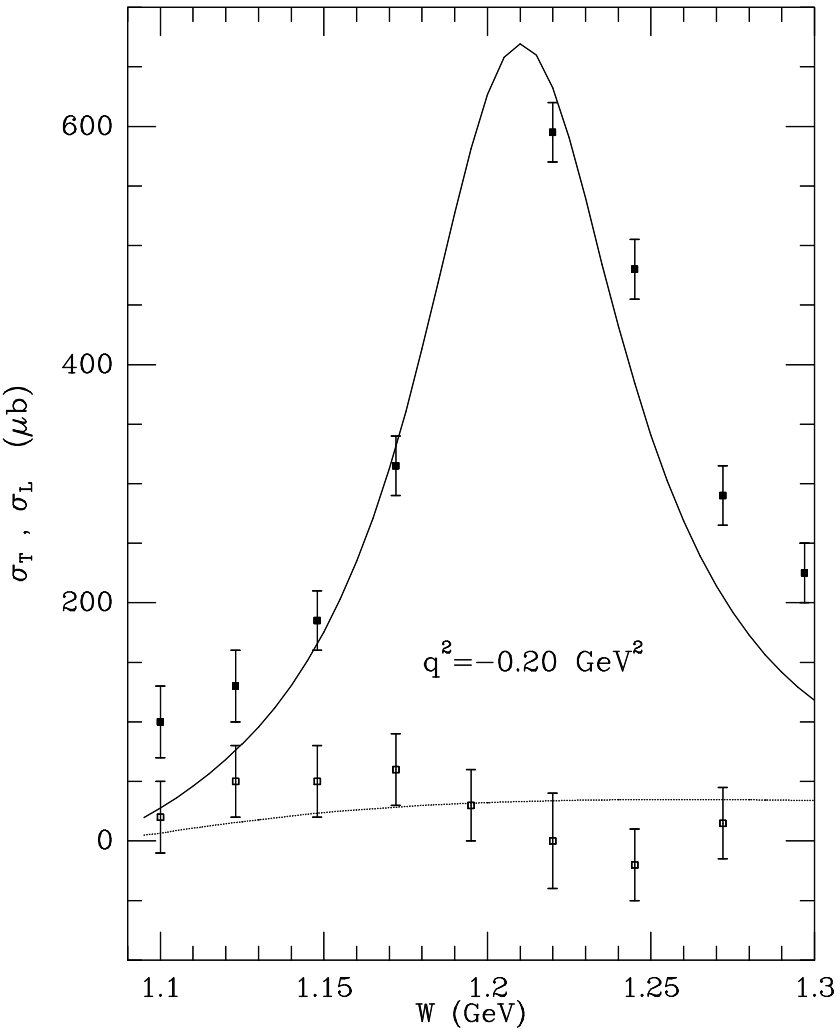

Fig.3.5 $W = \sqrt{s}$ dependence of the longitudinal (lower line) and transverse (upper line) cross sections summing over the final charge of the pion and integrating over Ω_π^*. Experimental data from [61].

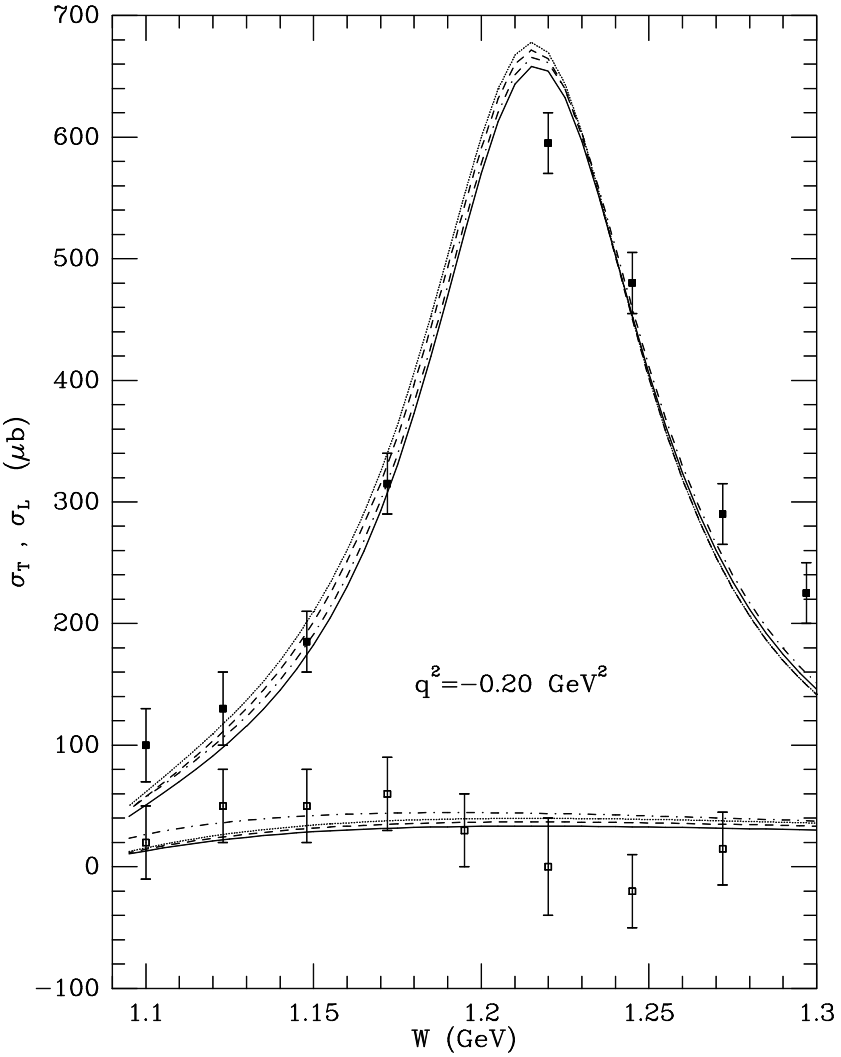

Fig.3.6 Inclusive cross sections σ_T and σ_L obtained: by using F_A and taking $F_1^p = F_{\gamma\pi\pi} = F_A$ (dotted lines); by using $F_{\gamma\pi\pi}$ and taking $F_1^p = F_A = F_{\gamma\pi\pi}$ (dash lines); by using F_1^p and taking $F_A = F_{\gamma\pi\pi} = F_1^p$ (full lines) and, finally, by using F_A, $F_{\gamma\pi\pi}$ and F_1^p (dash-dotted lines). Experimental data from [61].

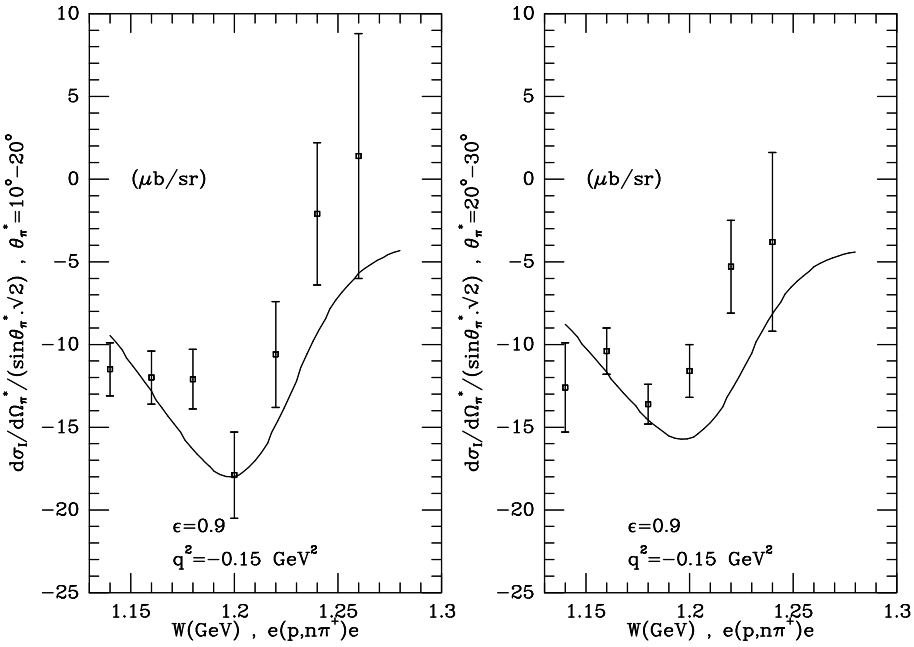

Fig.3.7 Calculation of $d\sigma_I/d\Omega_\pi^*/(\sin\theta_\pi^*\sqrt{2})$ in the $ep \to en\pi^+$ channel . Experimental data from [62].

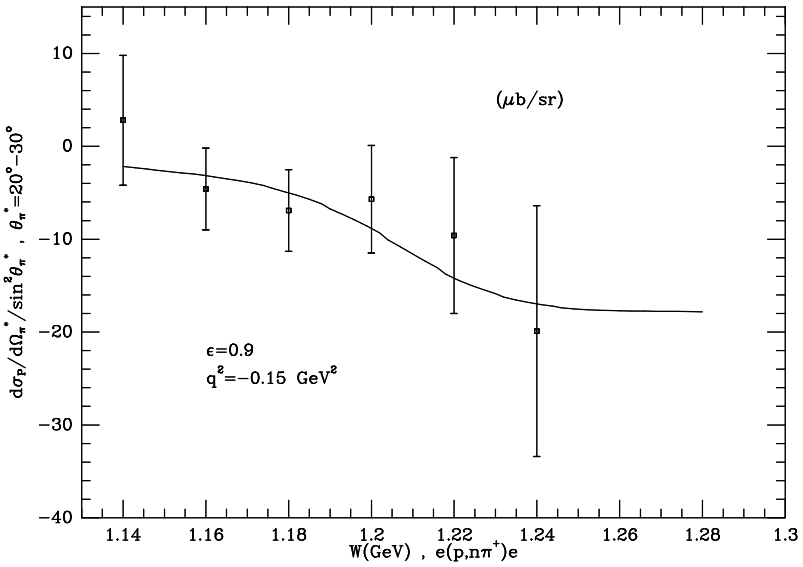

Fig.3.8 Calculation of $d\sigma_P/d\Omega_\pi^*/\sin^2\theta_\pi^*$ in the $ep \to en\pi^+$ channel. Experimental data from [62].

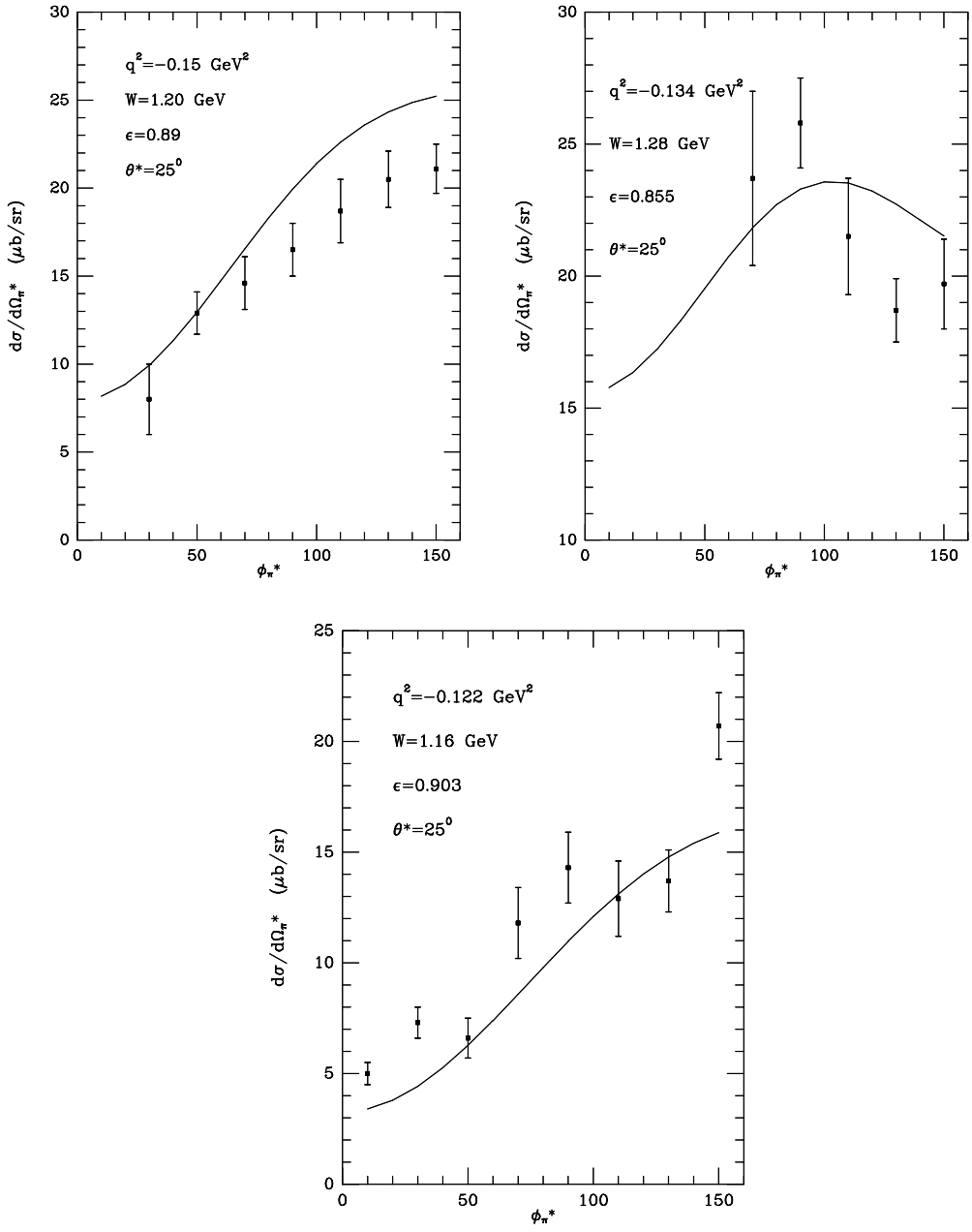

Fig.3.9 Calculation of the Φ_π^* dependence of the cross section in the $ep \to en\pi^+$ channel. Experimental data from [62].

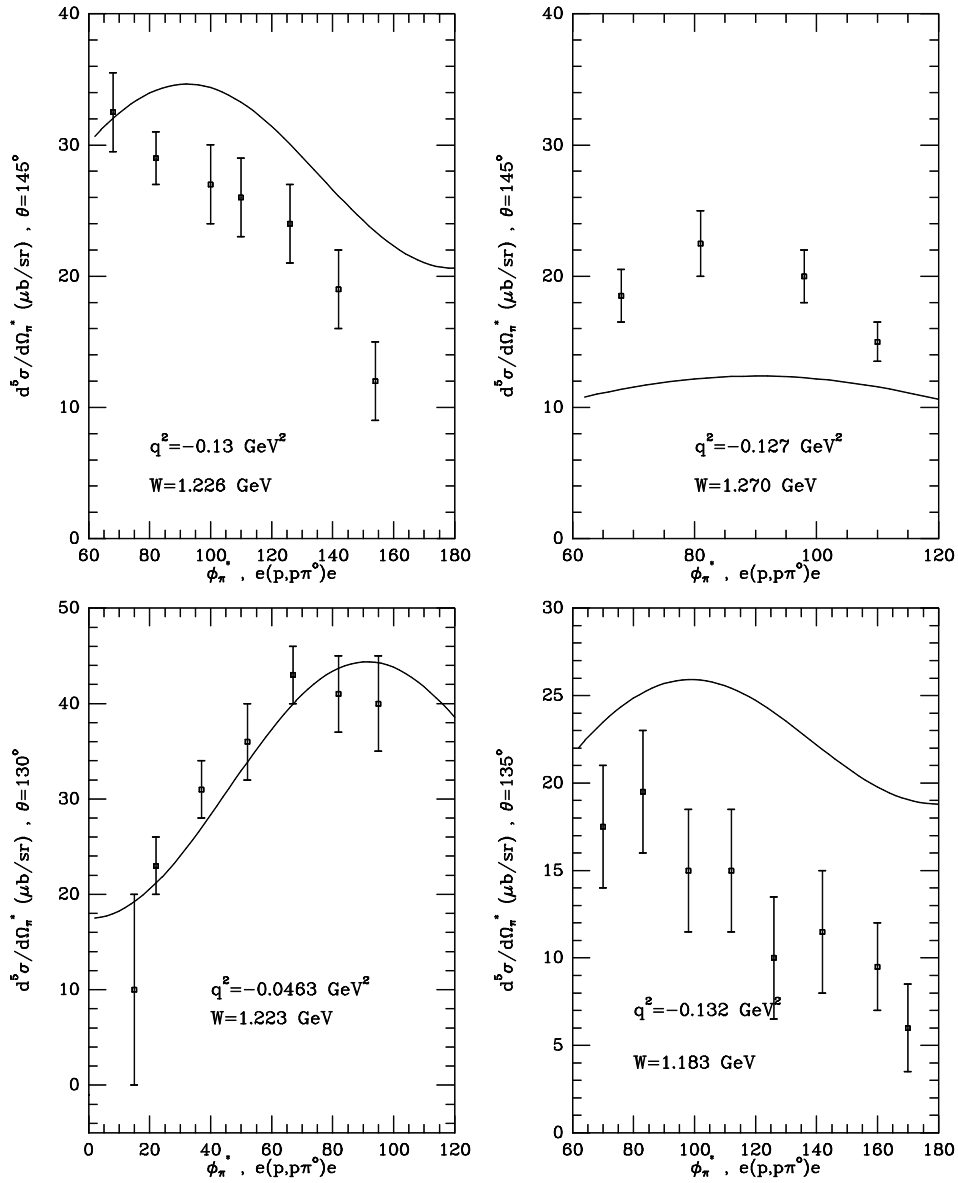

Fig.3.10 Calculation of the Φ_π^* dependence of the cross section in the $ep \to en\pi^0$ channel. Experimental data from [63].

In the next sections we shall use this model to evaluate the pion production contribution to the (e, e') cross section, as well as the exchange currents which contribute to the $2N$ emission channel.

4 The (e, e') reaction in nuclei.

4.1 Formalism

We want to use a covariant many body formalism to evaluate the (e, e') cross section. For this purpose we evaluate the electron self-energy for an electron moving in infinite nuclear matter. Diagrammatically this is depicted in fig. 4.1

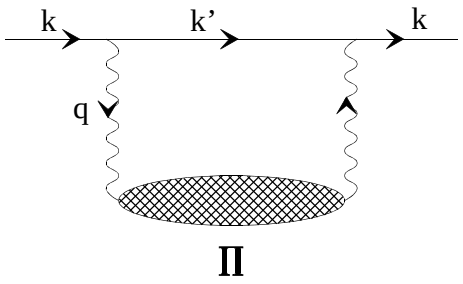

Fig.4.1 Diagrammatic representation of the electron self-energy in nuclear matter.

The electron disappears from the elastic flux, by inducing $1p1h, 2p2h...$ excitations or creating pions, etc., at a rate given by

$$\Gamma(k) = -2\frac{m_e}{E_e} Im\Sigma. \tag{20}$$

where $Im\Sigma$ is the imaginary part of the electron self-energy. This latter magnitude can be readily evaluated from the diagram of fig. 4.1 and we find:

$$\Sigma_r(k) = ie^2 \int \frac{d^4q}{(2\pi)^4} \bar{u}_r(k)\gamma_\mu \frac{(\not{k}' + m_e)}{k'^2 - m_e^2 + i\epsilon}\gamma_\nu u_r(k) \frac{\Pi_\gamma^{\mu\nu}(q)}{(q^2 + i\epsilon)^2} \tag{21}$$

where $\Pi_\gamma^{\mu\nu}$ is the virtual photon self-energy. Eq.(21) displays explicitly the electron propagator (fraction after γ_μ) and the photon propagator $(q^2 + i\epsilon)^{-1}$ which appears twice. By averaging over the spin of the electron, r, we find

$$\Sigma(k) = \frac{ie^2}{2m_e} \int \frac{d^4q}{(2\pi)^4} \frac{L_{\mu\nu}\Pi_\gamma^{\mu\nu}(q)}{q^4} \frac{1}{(k'^2 - m_e^2 + i\epsilon)} \tag{22}$$

and since we are interested in the imaginary part of Σ we can obtain it by following the prescription of the Cutkosky's rules. In this case we cut with a straight horizontal line the intermediate e' state and those implied by the photon polarization (shaded region). Those states are then placed on shell by taking the imaginary part of the propagator, self-energy, etc. Technically the rules to obtain $Im\Sigma$ reduce to making the substitutions:

$$\begin{aligned} \Sigma(k) &\to 2iIm\Sigma(k)\Theta(k^0) \\ \Xi(k') &\to 2iIm\Xi(k')\Theta(k'^0) \\ \Pi^{\mu\nu}(q) &\to 2iIm\Pi^{\mu\nu}(q)\Theta(q^0) \end{aligned} \tag{23}$$

where

$$\Xi(k') = \frac{1}{k'^2 - m_e^2 + i\epsilon} \tag{24}$$

and Θ is the Heaviside, or step, function. By proceeding according to these rules we obtain

$$Im\Sigma(k) = \frac{2\pi\alpha}{m_e}\int \frac{d^3q}{(2\pi)^3}\left(Im\Pi_\gamma^{\mu\nu}L_{\mu\nu}(k,k')\right)\frac{1}{q^4}\frac{1}{2E_e(\vec{k}')}\Theta(q^0) \tag{25}$$

The relationship of $Im\Sigma$ to the (e,e') cross section is easy: $\Gamma dtdS$ provides a probability times a differential of area, which is a contribution to a cross section. Hence we find

$$d\sigma = \Gamma(k)dtdS = -\frac{2m}{E_e}Im\Sigma dl\, dS = -\frac{2m}{|\vec{k}\,|}Im\Sigma d^3r \tag{26}$$

and hence the nuclear cross section is given by

$$\sigma = -\int d^3r\frac{2m}{|\vec{k}\,|}Im\Sigma(k,\rho(\vec{r})) \tag{27}$$

where we have substituted Σ as a function of the nuclear density at each point of the nucleus and integrate over the whole nuclear volume. Eq. (27) assumes the local density approximation, which, as shown in [32], is an excellent approximation for volume processes like here, hence we are neglecting the electron screening and using implicitly plane waves for the electrons (corrections to account for the small distortion are usually done in the experimental analysis of the data, see [64]).

Coming back to eq. (25) we find then

$$\frac{d^2\sigma}{d\Omega_e' dE_e'} = -\frac{\alpha}{q^4}\frac{|\vec{k}'|}{|\vec{k}|}\frac{1}{(2\pi)^2}\int d^3r\left(Im\Pi_\gamma^{\mu\nu}L_{\mu\nu}\right) \tag{28}$$

which gives us the (e,e') differential cross section in terms of the imaginary part of the photon self-energy.

If one compares eq. (28) with the general expression for the inclusive (e,e') cross section [71, 72] (see also eq. (11))

$$\frac{d^2\sigma}{d\Omega_e' dE_e'} = \frac{\alpha^2}{q^4}\frac{|\vec{k}'|}{|\vec{k}|}L^{\mu\nu}W_{\mu\nu} \tag{29}$$

we find

$$W^{\mu\nu} = -\frac{1}{\pi e^2}\int d^3r\frac{1}{2}\left(Im\Pi^{\mu\nu} + Im\Pi^{\nu\mu}\right) \tag{30}$$

Once again, by choosing $\vec{q}$ in the z direction and using gauge invariance one can write the cross section in terms of the longitudinal and transverse structure functions W_L, W_T as

$$\frac{d^2\sigma}{d\Omega_e' dE_e'} = \left(\frac{d\sigma}{d\Omega}\right)_{Mott}\left(-\frac{q^2}{|\vec{q}|^2}\right)\left\{W_L(\omega,|\vec{q}|) + \frac{W_T(\omega,|\vec{q}|)}{\epsilon}\right\} \tag{31}$$

where

$$q^2 = \omega^2 - |\vec{q}|^2$$

$$\left.\frac{d\sigma}{d\Omega}\right|_{Mott} = \frac{\alpha^2 \cos_e^2(\theta/2)}{4E_e^2 \sin_e^4(\theta/2)} \tag{32}$$

and

$$W_L = -\frac{q^2}{\omega^2} W^{zz} = -\frac{q^2}{|\vec{q}|^2} W^{00}$$
$$W_T = W^{xx} \tag{33}$$

Hence using eq. (30) we can write W_L and W_T in terms of the photon self-energy as

$$W_L = \frac{q^2}{\pi e^2 |\vec{q}|^2} \int d^3r Im\Pi^{00}(q, \rho(\vec{r}))$$
$$W_T = -\frac{1}{\pi e^2} \int d^3r Im\Pi^{xx}(q, \rho(\vec{r})) \tag{34}$$

where we see that we only need the components Π^{00} and Π^{xx}.

4.2 The virtual photon self-energy in pion production

We must construct a self-energy diagram for the photon which contains pion production in the intermediate states. This is readily accomplished by taking any generic diagram of the $\gamma^* N \to \pi N$ amplitude of fig. 3.2 and folding it with itself. One gets then the diagram of fig. 4.2 where the circle stands for any of the 6 terms of the elementary model for $\gamma^* N \to \pi N$. The lines going up and down in fig. 4.2. follow the standard many body nomenclature and stand for particle and hole states respectively.

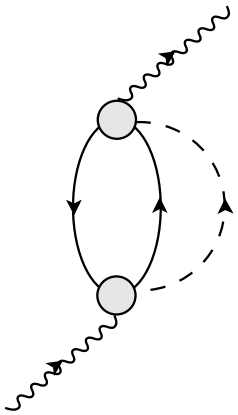

Fig.4.2 Photon self-energy obtained by folding the $\gamma^* N \to \pi N$ amplitude.

The photon self-energy corresponding to this diagram (actually 36 diagrams) is readily evaluated and gives

$$\Pi^{\mu\nu}_{NN'}(q) = i\int \frac{d^4k}{(2\pi)^4} \quad 2\int \frac{d^3p}{(2\pi)^3}\frac{n_N(p)[1-n_{N'}(p+q-k)]}{q^0-k^0+E(p)-E(p+q-k)+i\epsilon}\times$$
$$\times D_\pi(k)\tfrac{1}{2}Tr^{Spin}(T^\mu T^{\dagger\nu})_{NN'} \tag{35}$$

where T^μ is the amplitude for $\gamma^* N \to \pi N$. The indices N, N' in eq. (35) stand for the hole and particle nucleon states respectively and $n_N(\vec{p})$ is the occupation number in the Fermi local sea. $E(\vec{p})$ is the energy of the nucleon $\sqrt{\vec{p}^{\,2}+M_N^2}$ and D_π is the pion propagator

$$D_\pi(k) = \frac{1}{k^2-m_\pi^2+i\epsilon} \tag{36}$$

A further simplification can be done by evaluating the T^μ amplitudes at an average Fermi momentum. Explicit integration over $\vec{p}$ and also this approximation were done is [32] and the approximation was found to be rather good. We take $<\vec{p}>=\sqrt{\frac{3}{5}}k_F$ with k_F the local Fermi momentum $(3\pi^2\rho(r)/2)^{1/3}$ and a direction orthogonal to that of the virtual photon. The errors induced by this approximation are smaller than 5%. Then we can use the Lindhard function $\bar{U}_{N,N'}$ defined as

$$\bar{U}_{r,s}(q-k) = 2\int \frac{d^3k}{(2\pi)^3}\frac{n_r(\vec{p})[1-n_s(\vec{p}+\vec{q}-\vec{k}\,)]}{q^0-k^0+E(\vec{p})-E(\vec{p}+\vec{q}-\vec{k}\,)+i\epsilon} \tag{37}$$

where the indices, r, s correspond to protons or neutrons.

For the evaluation of the imaginary part we need an extra Cutkosky rule

$$U(p) \to 2iImU(p)\Theta(p^0)$$

which is the general rule considering that the Lindhard function plays the role of a *ph* propagator.

Hence we apply the Cutkosky rules of eq. (23) and the former one and we find

$$Im\Pi^{\mu\nu} = \int \frac{d^3k}{(2\pi)^3} Im\bar{U}_{NN'}(q-k)\frac{1}{2\omega(\vec{k}\,)}\theta(q^0-\omega(\vec{k}\,))\times$$
$$\times\ \tfrac{1}{2}Tr^{Spin}(T^\mu T^{\dagger\nu}_{NN'})\Big|_{k^0=\omega(\vec{k}\,)} \tag{38}$$

Since there are analitycal expressions for $Im\bar{U}_{NN'}$ (see Appendix B of [32]), the approximation done saves us three integrals and a considerable amount of computational time.

There is an interesting test to eq.(38). Indeed, in the limit of small densities the Pauli blocking factor $1-n$ becomes 1 and $Im\bar{U}_{NN'}(q) \simeq -\pi\rho_N\delta(q^0-\frac{\vec{q}^{\,2}}{2M_N})$. Substituting this into eq. (38) and (29),(30) one easily obtains that $\sigma_{eA} = \sigma_{ep}Z + \sigma_{en}N$, the strict impulse approximation. By performing the integral in eq. (38) one accounts for Pauli blocking and in an approximate way for Fermi motion. Later on we shall introduce other corrections due to medium polarization.

4.3 The Δ excitation term

One of the terms implicit in eq. (38) is the one where one picks up the Δ excitation term both in T^{μ} and is $T^{\dagger\nu}$. This term is depicted diagrammatically in fig. 4.3(a) and, like in pion-nuclear and photo-nuclear reactions at intermediate energies, plays a major role in this reaction.

In order to evaluate this piece one can go back to eq. (35) and perform the d^4k integration to factorize the Δ width and on the other hand one will also have the modulus squared of the Δ propagator present in the Δ term of eq. (5). This, however, can be obtained more economically by reinterpreting the diagram 4.3 (a) as a Δh excitation with a Δ width. We can also divert a little from the general formulation, and in order to gain some extra accuracy we can implement Lorentz covariance exactly simply boosting the tensor $\Pi^{\mu\nu}$ from a frame where the Δ is at rest ($\vec{q}+\vec{p}=\vec{p}_{\Delta}=0$), where the amplitude of eq. (5) would be (by construction) equivalent to the relativistic amplitude.

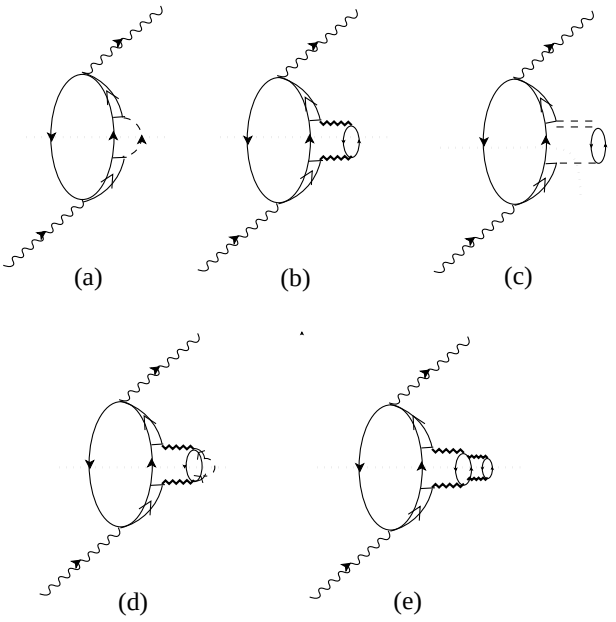

Fig.4.3 Diagrammatic representation of the Δh photonuclear excitation piece.

Hence we get

$$\begin{aligned} Im\Pi^{\mu\nu}_{\Delta} = \; & \textstyle\sum_{ij} |c_{ij}|^2 \frac{f^2_{\gamma}(q^2)}{m^2_{\pi}} \int \frac{d^3p}{(2\pi)^3} n_i(p) \Lambda^{\mu}_{m}(p,q) \Lambda^{\nu}_{l}(p,q) \\ & \times Tr\left((\vec{S}^{\dagger} \times \vec{q}_{cm})^m (\vec{S} \times \vec{q}_{cm})^l \right) \frac{s}{M^2_{\Delta}} \times \\ & \times \frac{Im\Sigma^j_{\Delta}(p+q) - \dfrac{\bar{\Gamma}}{2}(p+q)}{\left| \sqrt{s} - M_{\Delta} + i\dfrac{\bar{\Gamma}(s)}{2} - \Sigma_{\Delta}(s) \right|^2} \end{aligned} \tag{39}$$

The Lorentz matrix Λ is such that $\Lambda^{\mu}_{\gamma\nu} q^{\nu}_{cm} = q^{\mu}$ and $s = (p+q)^2$. The coefficients

C_{ij}, $i,j = 1,2$ stands for proton or neutron, account for isospin and are given by

$$|C_{ij}| = \left(\frac{2}{3}\right)^2 \delta_{ij} + \frac{2}{9}\delta_{i,j+1} + \frac{2}{9}\delta_{i,j-1} \tag{40}$$

Eq. (39), however, seems to neglect the Pauli blocking factor $1-n$ of eq. (35). This factor, however, is taken into account implicitly and leads to the Pauli blocked width $\bar{\Gamma}$, which is evaluated in [69]. Furthermore, in a nuclear medium the Δ is renormalized and acquires a self-energy Σ_Δ, which is also accounted for in eq.(39). The results of [51] for Σ_Δ are used in the calculation. This self-energy accounts for the diagrams depicted in fig. 4.3, where the double dashed line stands for the effective spin -isospin interaction, while the serrated line accounts for the induced interaction. The effective spin-isospin interaction is originated by a pion exchange in the presence of short range correlations and includes ρ-exchange as well. It is obtained by substituting

$$\hat{q}_i\hat{q}_j D_\pi(q) \rightarrow \hat{q}_i\hat{q}_j V_l(q) + (\delta_{ij} - \hat{q}_i\hat{q}_j)V_t(q) \tag{41}$$

and expressions for V_l, V_t are found in [51] ($(f_{\pi NN}/m_\pi)^2 V_{l,t}$ here is equivalent to $V_{l,t}$ of [51]). The induced interaction accounts for the series of diagrams depicted in fig. 4.4.

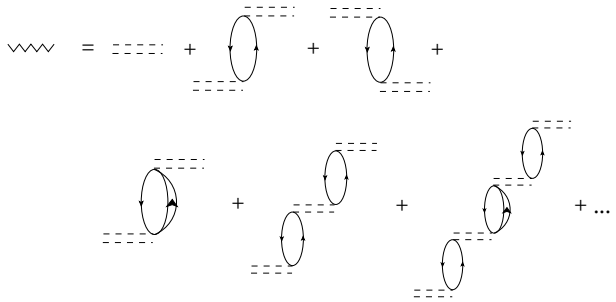

Fig.4.4 Feynman diagrams included in the evaluation of the Δ self-energy.

There is an RPA sum through ph and Δh excitation and is readily obtained as

$$\begin{aligned} V_{ind} \;=\; & \hat{q}_i\hat{q}_j \frac{V_l(q)}{1 - U(q)V_l(q)\left(\frac{f_{\pi NN}}{m_\pi}\right)^2} + \\ & (\delta_{ij} - \hat{q}_i\hat{q}_j)\frac{V_t(q)}{1 - U(q)V_t(q)\left(\frac{f_{\pi NN}}{m_\pi}\right)^2} \end{aligned} \tag{42}$$

where now $U(q) = U_N(q) + U_\Delta(q)$ is the Lindhard function for $ph + \Delta h$ excitations including forward going and backward going bubbles [51] in contrast to $\bar{U}$ which only contains the forward going bubble of a ph excitation (the only one which contributes to ImU_N for $q^0 > 0$). U_N in addition incorporates a factor two of isospin with respect to $\bar{U}$, such that $ImU_N = 2Im\bar{U}$ for symmetric nuclear matter. However, all the work which goes into the evaluation of Σ_Δ is done in ref. [51], where a useful analytical parameterization of the numerical results is given that we use here. The imaginary part is parametrized as

$$Im\Sigma_\Delta = -\left\{C_Q(\rho/\rho_0)^\alpha + C_{A_2}(\rho/\rho_0)^\beta + C_{A_3}(\rho/\rho_0)^\gamma\right\} \tag{43}$$

where the different coefficients are given in [51] as a function of the energy.

The separation of terms in eq. (43) is useful because the term C_Q comes from the diagrams (c) and (d) of fig. 4.3 when the lines cut by the dotted line are placed on shell, and hence the term is related to the (γ^*, π) channel, while C_{A2}, C_{A3} come from the diagrams (b) and (e) and are related to two and three body absorption. Hence, the separation in this formula allows us to separate the final cross section into different channels.

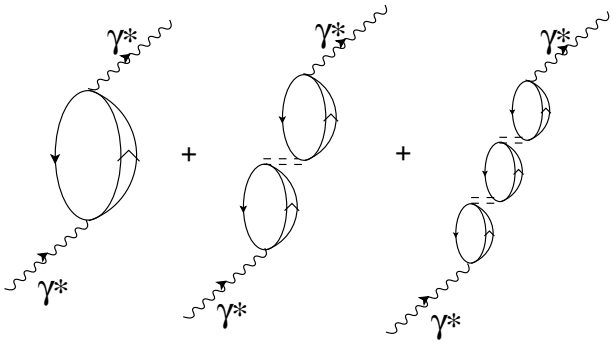

Fig.4.5 Irreducible pieces in the Δh channel from the Δh interaction.

It is also easy to realize that the RPA sum of Δh excitations, shown in fig. 4.5, can be taken into account by substituting $Re\Sigma_\Delta$ by [32]

$$Re\Sigma_\Delta \to Re\Sigma_\Delta + \frac{4}{9}\left(\frac{f^*}{m_\pi}\right)^2 \rho V_t \tag{44}$$

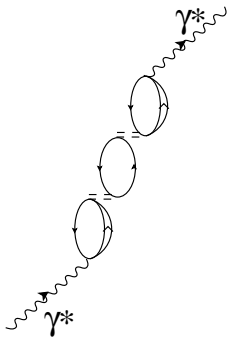

Fig.4.6 Diagrammatic representation of the inclusion of a ph excitation between Δh excitations.

and furthermore, if we wish to include some ph excitation in between, see fig. 4.6, (which is actually not relevant numerically), this is done easily by substituting $Re\Sigma_\Delta$ by

$$Re\Sigma_\Delta + \frac{4}{9}\left(\frac{f^*}{m_\pi}\right)^2 \frac{V_t}{\left(1 - \frac{f^2_{\pi NN}}{m^2_\pi} U_N V_t\right)} \rho \tag{45}$$

4.4 Results for the Δ contribution

In fig. 4.7 we show the results coming from the Δ term discussed in the former section. The experimental data are coming from [3]. We have separated the contribution from the different channels. Besides the upper solid line which stands for the total contribution, looking from up to down at about $\omega = 350$ MeV the next line corresponds to pion production, the following one is two nucleon absorption and the lowest one three body absorption. We can see that most of the experimental strength in the Δ region is provided by this Δ excitation term, but there is still some strength missing. In fig. 4.8 we show the contribution of the delta piece for the ^{208} Pb nucleus. The data are now from [73]. The results are similar to those found in ^{12}C and there is still some strength missing. The study of this missing strength will occupy the next sections.

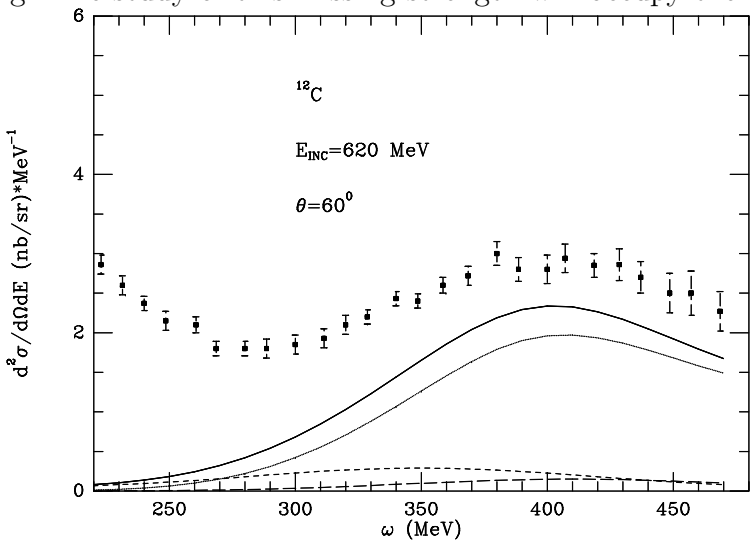

Fig.4.7 Contribution of the Δ piece to the (e, e') cross section in ^{12}C. Experimental data from [3]. See text for different contributions.

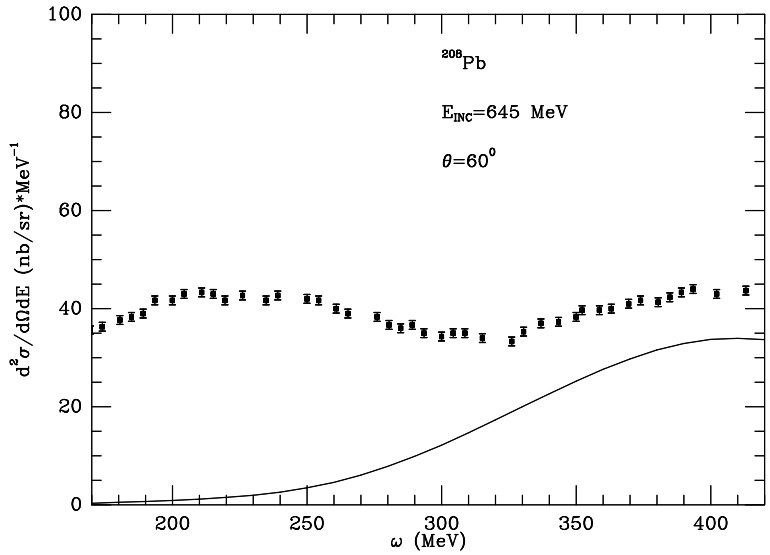

Fig.4.8 Contribution of the Δ piece to the (e, e') cross section in ^{208}Pb. Experimental data from [73].

4.5 Two body photoabsorption

Let us go back to the generic diagram of pion electroproduction of fig. 4.2. Let us take the pion line and allow the pion to excite a ph. This leads us to the diagram of fig. 4.9.

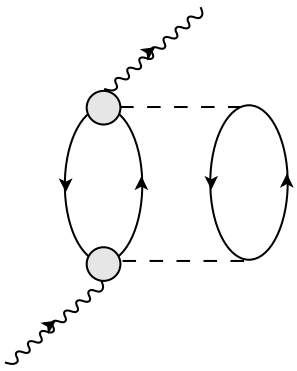

Fig.4.9 Photon self-energy obtained from the one in fig. 4.2 when the pion is allowed to excite a ph.

This is still a generic diagram which actually contains 36 diagrams when in the shaded circle we put each one of the terms of the $\gamma^* N \to \pi N$ amplitude of fig. 3.2. One must avoid the temptation of factorizing these amplitudes in order to evaluate these diagrams since some of them might be symmetric and then have a symmetry factor 1/2. This is the case here with one diagram implicit in fig. 4.9, which is the one corresponding to the pion pole term in each one of the $\gamma^* N \to \pi N$ amplitudes. This diagram is shown explicitly in fig. 4.10.

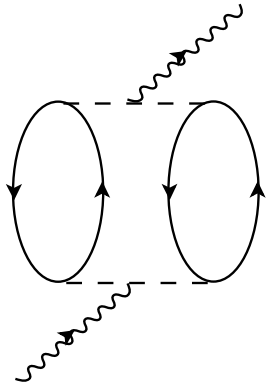

Fig.4.10 Pion pole term included in fig. 4.9.

One can see that the diagrams in fig. 4.9 contribute to $Im\Pi$ according to Cutkosky rules when we cut by a horizontal line and the $2p2h$ are placed on shell.

The contribution of the diagram of fig. 4.9 is readily done. We obtain

$$\Pi^{(2)\mu\nu}(q) = \sum_{N,N'} i \int \frac{d^4k}{(2\pi)^4} \frac{d^3p}{(2\pi)^3} \frac{n_N(p)[1-n_{N'}(p+q-k)]}{q^0 - k^0 + E(p) - E(p+q-k) + i\epsilon} \times \tag{46}$$

$$D_\pi^2(k) \frac{f_{\pi NN}^2}{m_\pi^2} \vec{k}^2 U_\lambda(k) Tr^{Spin}(T^\mu T^{\dagger\nu})_{NN'} S_\alpha F_\pi^4(k)$$

where U_λ is the Lindhard function for ph by an object of charge λ: this is, twice $\bar{U}_{p,n}$ or $\bar{U}_{p,n}$ for the excitation by a charged pion or $\bar{U}_{p,p} + \bar{U}_{n,n}$ for the excitation by a neutral pion and $\vec{k}$ is the pion momentum. The factor $F_\pi^4(k)$, where F_π is the pion form factor appears because now the pions are off shell. Recall that we also take all form factors equal in order to preserve gauge invariance (eq. (9)). The factor S_α is the symmetry factor, unity for all diagrams and 1/2 for the symmetric one of fig. (4.10).

We can again simplify the expression by taking an average nucleon momentum of the Fermi sea to evaluate the matrix elements of $T^\mu\, T^{\dagger\nu}$. This allows us to factorize the Lindhard function and we get

$$\begin{aligned}\Pi^{(2)\ \mu\nu}(q) = \ & \sum_{NN'} i \int \frac{d^4k}{(2\pi)^4} \bar{U}_{NN'}(q-k) D_\pi^2(k) \frac{f_{\pi NN}^2}{m_\pi^2} \\ & \vec{k}^2 U_\lambda(k) \tfrac{1}{2} Tr^{Spin}(T^\mu T^{\dagger\nu})_{NN'} S_\alpha F_\pi^4(k)\end{aligned} \tag{47}$$

By applying Cutkosky rules we find

$$\begin{aligned}Im\Pi^{(2)\ \mu\nu} = \ & -\sum_{NN'} \int \frac{d^4k}{(2\pi)^4} \Theta(q^0-k^0) Im\bar{U}_{NN'}(q-k) \Theta(k^0) \times \\ & Im U_\lambda(k) D_\pi^2(k) \frac{f_{\pi NN}^2}{m_\pi^2} \vec{k}^2 F_\pi^4(k) S_\alpha \times \\ & Tr^{Spin}(T^\mu T^{\dagger\nu})_{NN'}\end{aligned} \tag{48}$$

The cut which places the two ph on shell in the diagrams of fig. 4.9 is not the only possible one. In fig. 4.11 we show a different cut (dotted line) which places one ph and the pion on shell.

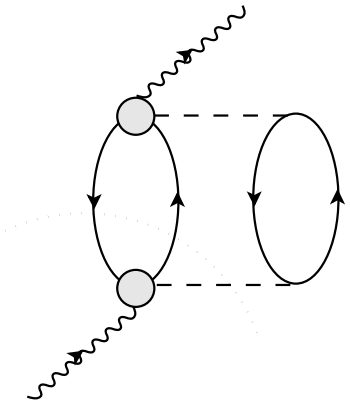

Fig.4.11 Same as fig. 4.9 and showing the cut which places one ph and the pion on shell.

This contribution is taken into account in the Δ excitation term by means of the term C_Q. As done for real photons in [32], we neglect this contribution in the other terms, because at low energies where the background pieces are important, the (γ^*, π) channel is small and at high energies where the (γ^*, π) contribution is important, this channel is dominated by the Δ excitation and there this correction is taken into account.

We have also considered two body diagrams where each photon couples to different bubbles: As found is [32] only one of them is relevant, the one in fig. (4.12), which involves the KR term alone and which we take into account.

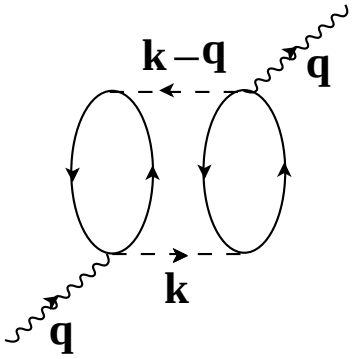

Fig.4.12 Feynman diagram related to the KR term of fig. 4.9 with outgoing photon from the second nucleon.

Following the same rules as above, this term is readily evaluated and gives

$$
\begin{aligned}
Im\Pi^{00} = \; & -2e^2\left(\frac{f^2}{m_\pi^2}\right)^2 2F_A^2(q^2)\times \\
& \int\frac{d^4k}{(2\pi)^4}D_0(k)D_0(k-q)\frac{(\vec{k}\vec{q})(\vec{k}-\vec{q})\vec{q}}{M_N^2}\times \\
& F^2_{\pi NN}(k)F^2_{\pi NN}(k-q)\times \\
& \Big[Im\bar{U}_{pp}(q)Im\bar{U}_{pp}(k-q)+Im\bar{U}_{pn}(q)Im\bar{U}_{np}(k-q)+ \\
& +Im\bar{U}_{np}(q)Im\bar{U}_{pn}(k-q)\Big]\,\Theta(k^0)\Theta(k^0-q^0)
\end{aligned}
\tag{49}
$$

$$
\begin{aligned}
Im(\Pi^{xx}+\Pi^{yy}) = \; & -2e^2\left(\frac{f^2}{m_\pi^2}\right)^2 2F_A^2(q^2)\times \\
& \int\frac{d^4k}{(2\pi)^4}D_0(k)D_0(k-q)|\vec{k}|^2 sin^2\theta F^2_{\pi NN}(k)F^2_{\pi NN}(k-q)\times \\
& \Big\{\frac{1}{2}\left(\frac{q^0}{M_N}\right)^2 Im\bar{U}_{pp}(q)Im\bar{U}_{pp}(k-q)+
\end{aligned}
$$

$$\left[-\left(1-\frac{q^0}{2M}\right)\sqrt{2}\right]^2 Im\bar{U}_{pn}(q)Im\bar{U}_{np}(k-q)$$

$$+\left[\left(1+\frac{q^0}{2M}\right)\sqrt{2}\right]^2 Im\bar{U}_{np}(q)Im\bar{U}_{pn}(k-q)\Bigg\}\times \tag{50}$$

$$\Theta(k^0)\Theta(k^0-q^0)$$

The contribution of this term is roughly 1/2 of the $KR\times KR$ term in the generic diagram of fig. 4.9.

4.6 Contributions tied to the $(\gamma^*, 2\pi)$ channel

The $\gamma N\to\pi\pi N$ reaction has been the subject of recent detailed experimental analyses [74, 75] and also of recent theoretical analyses, some of them spanning a large energy range [76, 77] and others concentrating only very close to threshold in order to test predictions of chiral perturbation theory [78, 79].

The model in ref. [76] for the $\gamma p\to\pi^+\pi^- p$ uses 67 Feynman diagrams, while ref. [77], where the model is extended to the other isospin channels uses only 20 diagrams which are necessary below $E_\gamma = 800\,MeV$, where the new data have been measured.

Although the model is rather elaborate and contains many terms, one can see that the gross features of the reaction can be obtained with the two terms of fig. 4.13, accounting for about 80% of the cross section.

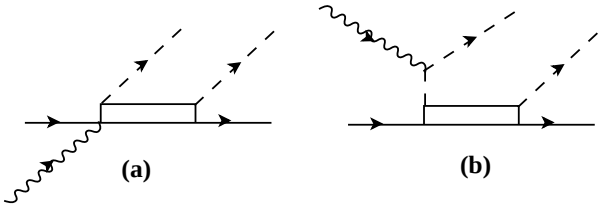

Fig.4.13 Relevant Feynman diagrams that enter in the evaluation of the $\gamma^*N\to N2\pi$ cross section.

Since here we are only concerned about corrections to the more important terms which we have discussed above, it is sensible to just take these two diagrams. The diagram in fig. (a) is the $\Delta N\pi\gamma$ Kroll Ruderman (KR) term, while the one in fig. (b) is the pion pole term. In both terms the Δ is excited. The KR term, which appears from the $\Delta N\pi$ vertex by minimal coupling, is given by,

$$\mathcal{M}^\mu = \left\{\begin{array}{ccc} 0 & , & \pi^0 \\ 1 & , & \pi^\pm \end{array}\right\}\left(e\frac{f^*}{m_\pi}\right)\times$$

$$\left(1\tfrac{1}{2}\tfrac{3}{2}\,|m_\pi M_N M_\Delta\right)\left(\begin{array}{c} \frac{\vec{S}^\dagger\vec{p}_\Delta}{\sqrt{s}} \\ \\ \vec{S}^\dagger \end{array}\right) \tag{51}$$

corresponding to $\pi^{\pm}\Delta$ production in the $\gamma^* N \to \Delta\pi$ vertex.

By following the same steps as before we obtain the many body diagrams of fig. (4.14), where the dashed circle indicates any of the two terms of fig. 4.13.

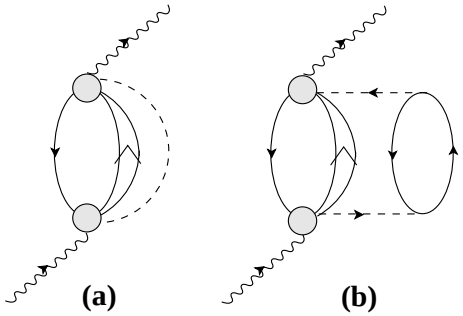

Fig.4.14 Photon self-energy diagrams obtained by folding the terms of fig. 4.13. Diagram (b) is obtained when the pion is allowed to produce a ph excitation.

Furthermore, as discussed in ref. [32], in the diagrams of fig. 4.14 (b) we keep only the term with the $KR \times KR$ in the vertices. This is done since the pion in flight term, can be considered as a two step process of a $\gamma^* N \to \pi N$ with π, a real pion, followed by the $\pi N \to \Delta$ excitation. The two step processes redistribute strength but do not change the cross section and hence are not included in our approach.

Since the Δ in the Δh excitation in fig. 4.14 is also renormalized, we are accounting for the physical channels depicted in fig. 4.15 when placing on shell the states cut by the dotted line.

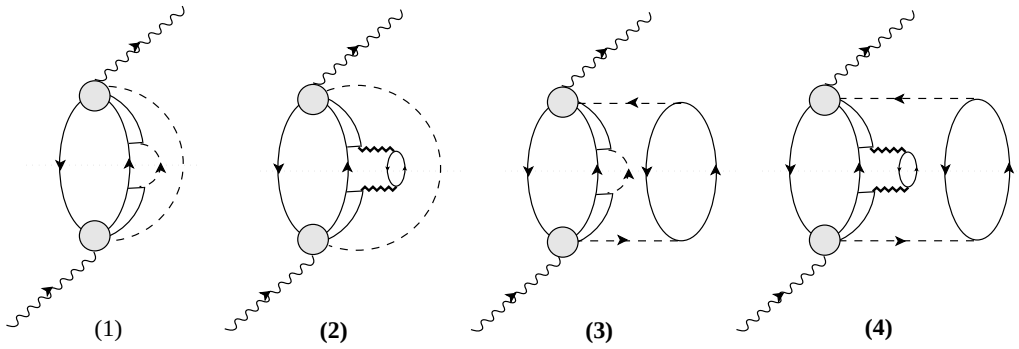

Fig.4.15 Detail of fig. 4.14 indicating the physical channels associated to the cuts.

As one can see there, (1) accounts for $1p1h\,2\pi$ excitation, (2) and (3) for $2p2h\,1\pi$ excitation and (4) for $3p3h$ excitation.

The evaluation of these pieces follows exactly the same steps as for figs. 4.2 and 4.9, simply replacing the $\gamma^* N \to \pi N$ by the $\gamma^* N \to \pi\Delta$ amplitudes and one nucleon propagator by the Δ propagator. The contribution of these terms below $\omega = 350\,MeV$ is very small. Their importance increases with the energy and at $\omega = 450\ MeV$ they account for about 1/5 of the cross section, as found for real photons.

4.7 Polarization (RPA) effects

In the diagrams of fig. 4.9 we can consider the ph as just the first order of a series of the RPA excitations through ph and Δh excitations. If one replaces the ph by the RPA series, one is led to the terms implicit in fig. 4.16. A similar series would appear for the case of the (γ, π) process depicted in fig. 4.2.

In practical terms this is done in a simple way by having a bookkeeping of both the spin longitudinal and spin transverse parts and replacing

$$ImU_N \to a\frac{ImU_N}{|1 - U_\lambda(q)V_l|^2} + b\frac{ImU_N}{|1 - U_\lambda V_t|^2} \tag{52}$$

where a, b measure the strength of the longitudinal and transverse parts.

For the transverse part of the photon self-energy Π^{xx}, Π^{yy} the procedure to follow is identical to the one explained in section 9 of [32] and we refer the reader to this paper (see also [58]). The only novelty here is Π^{00}, but this component is of spin longitudinal character and is renormalized by means of eq.(52) with $a = 1, b = 0$. In the Δ term the polarization effects are already included in the self-energy of ref. [51], hence, no further corrections are needed.

5 Short range correlations

So far the calculations have been done using implicitly plane waves for the nucleon states. Short range nuclear correlations modify the two nucleon relative wave function and this has a repercusion in some of the matrix elements which we have calculated. This is particularly true in those matrix elements which involve a p-wave coupling in the vertex for each of the two nucleons, because the pion exchange generates a $\delta(\vec{r})$ function, which is rended inoperative in the presence of short range correlations. This is not exactly the case if finite size effects by means of form factors are taken into account, but the need to implement the effects of the short range correlations remains. The correlations can also introduce spin transverse components in the p-wave-p-wave terms which were originally of the spin longitudinal nature [65]. Hence, at the same time that one introduces the effect of correlations, one takes advantage of this and introduces the ρ meson exchange in this case. In this way, we generated V_l and V_t of eq.(41).

The method to introduce the effects of correlations is to substitute a two nucleon amplitude $V(q)$ by

$$V(\vec{q}) \to \frac{1}{(2\pi)^3}\int d^3k V(\vec{k})\Omega(\vec{q} - \vec{k})$$

where $\Omega(\vec{p})$ is the Fourier transform of a nuclear correlation function.

Once again the techniques to make these corrections can be seen in [32] (appendix D, see also [58]), and we do not repeat them here.

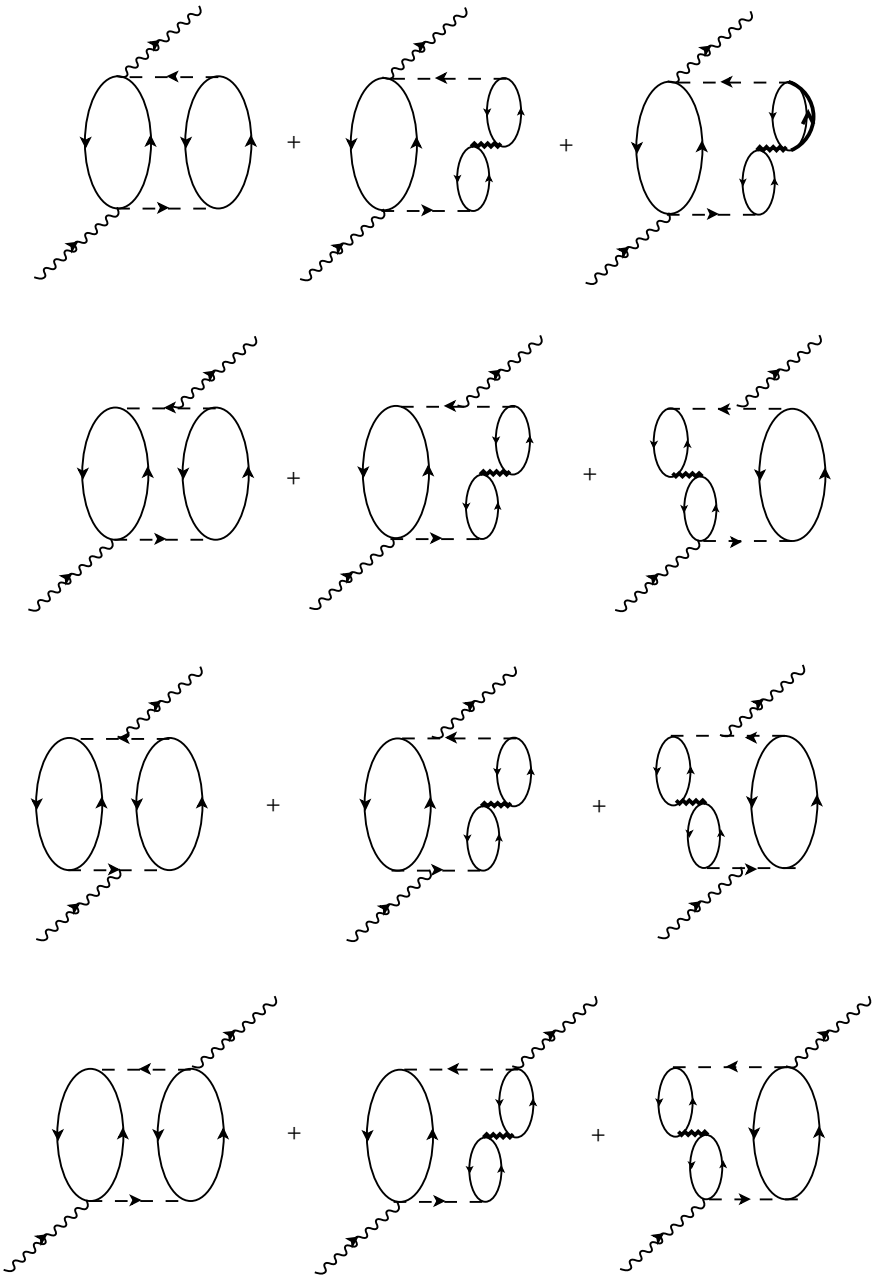

Fig.4.16 Terms of the KR and pion pole block implicit in fig. 4.9 showing the medium polarization through RPA ph and Δh excitations induced by the pion.

6 Detailed study of the quasielastic peak

6.1 Formalism

So far we have studied the (γ^*, π) process and the γ^* absorption by a pair or trio of particles. This was done keeping a parallelism to the real photon case. However, unlike the case with real photons, a virtual photon can be absorbed by one nucleon leading to the quasielastic peak of the response function. We have left this problem till the end in order to introduce the concepts of many body which proved relevant in the scattering of real photons with nuclei and in the equivalent channels of virtual photons studied before.

Then we can use the same concepts and ideas here in order to introduce the appropriate many body corrections to the quasielastic peak.

Thus we begin by evaluating $\Pi^{\mu\nu}$ for the $1ph$ excitation driven by the virtual photon, as depicted in fig. 6.1.

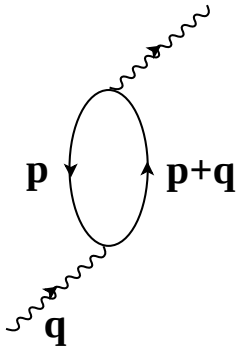

Fig.6.1 Photon self-energy diagram for the $1ph$ excitation driven by the virtual photon.

The photon self-energy associated to this diagram is given by

$$-i\Pi^{\mu\nu} = \int \frac{d^4p}{(2\pi)^4} \quad \frac{in_i(p)}{p^0 - E(\vec{p}) + i\epsilon} \times \\ \times \frac{i(1-n_j(p+q))}{p^0 + q^0 - E(\vec{p}+\vec{q}) - i\epsilon} Tr(V^\mu V^{\dagger\nu}) \tag{53}$$

where V^μ represents the γNN vertex and $E(\vec{p})$ is the nucleon kinetic energy. The vertex V^μ is given by

$$V^\mu = \bar{u}_r(\vec{p}) \left\{ eF_1\gamma^\mu - ie\frac{G_M}{2M_N}\mu_n\sigma^{\mu\rho}q_\rho \right\} u_{r'}(\vec{p}+\vec{q}) \tag{54}$$

Once again the application of Cutkosky rules leads to

$$Im\Pi^{00} = -\int \frac{d^3p}{(2\pi)^2} \quad n_i(p)(1-n_j(p+q)) \times \\ \times \delta(p^0 + q^0 - E(\vec{p}+\vec{q}\,))Tr(V^0 V^{\dagger 0}) \tag{55}$$

$$Im\Pi^{xx} = -\int \frac{d^3p}{(2\pi)^2} \quad n_i(p)(1-n_j(p+q))\times \\ \times\delta(p^0+q^0-E(\vec{p}+\vec{q})\,)Tr(V^xV^{\dagger x}) \tag{56}$$

and if we average $Tr(V^\mu V^{\dagger\nu})$ over the nucleon momentum in the Fermi sea we can write

$$Im\Pi^{00} = \frac{1}{2} Im\bar{U}(q,\rho)\langle Tr(V^0V^{\dagger 0})\rangle \tag{57}$$

$$Im\Pi^{xx} = \frac{1}{2} Im\bar{U}(q,\rho)\langle Tr(V^xV^{\dagger x})\rangle \tag{58}$$

The average over the Fermi momentum can be done keeping terms up to q^2/M_N^2 and we find in terms of

$$A^{\mu\nu} = \frac{1}{e^2} < Tr(V^\mu V^{\dagger\nu}) >$$

$$A^{00} = \frac{1}{M_N^2}\left\{ \frac{1}{1-\dfrac{q^2}{4M_N^2}} \left[G_E^2(q) - \frac{q^2}{4M_N^2} G_M^2(q) \right] \frac{1}{2}(2p^0+q^0)^2 - \frac{1}{2}\vec{q}^{\,2} G_M^2(q) \right\} \tag{59}$$

$$A^{xx} = \frac{1}{M_N^2}\left\{ \frac{1}{1-\dfrac{q^2}{4M_N^2}} \left[G_E^2(q) - \frac{q^2}{4M_N^2} G_M^2(q) \right] \frac{2}{5}k_F^2 - \frac{1}{2}q^2 G_M^2(q) \right\} \tag{60}$$

where $p^0 = M_N + \frac{3}{5}\frac{k_F^2}{2M_N}$ and G_E, G_M are the Sachs form factors [60, 71].

6.2 Spectral function description and final state interaction

One of the corrections to the bare *ph* excitation studied above is the one induced by final state interaction, as we indicated in section 2, which in our approach can be taken into account by dressing up the nucleon propagator of the particle state in the *ph* excitation, as depicted in fig. 6.2 (there the dashed line would account for the whole NN interaction not just pion exchange). However, some caution must be exerted when talking about this diagram.

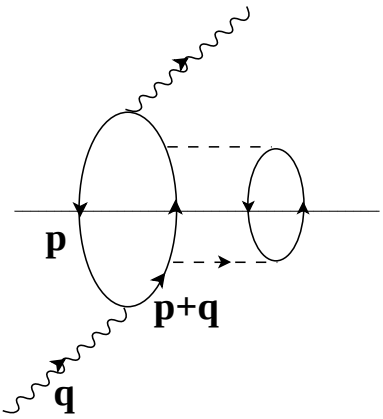

Fig.6.2 Photon self-energy diagram obtained from fig. 6.1 by dressing up the nucleon propagator of the particle state in the ph excitation.

In the first place, this is one of the terms implicit in the generic diagram of fig. 4.9 when the nucleon pole term is taken in each of the $\gamma^* N \to NN$ amplitudes. This term poses no problem for real photons and leads to a small fraction of the two nucleon absorption. However, for virtual photons this diagram is divergent. The reason is that when placing the $2p2h$ excitation on shell through Cutkosky rules, we still have the square of the nucleon propagator with momentum $p+q$ in the figure. This propagator can be placed on shell for virtual photons (not for real photons) and we get a divergence.

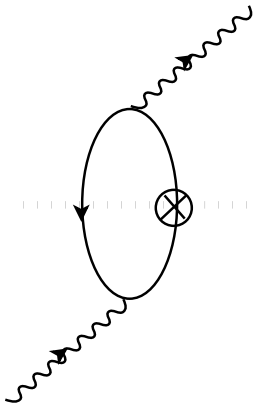

Fig.6.3 Insertion of the nucleon self-energy on the nucleon line of the particle state.

The divergence is physical in the sense that its meaning is the probability per unit time of absorbing a virtual photon by one nucleon times the probability of collision of the final nucleon with other nucleons in the infinite Fermi sea in the lifetime of this nucleon [66]. Since this nucleon is real, its lifetime is infinite and thus the probability infinite. The problem is physically solved [66] by recalling that the nucleon in the Fermi sea has a self-energy with an imaginary part which gives it a finite lifetime (for collisions). This is also immediately taken into account technically by iterating the nucleon self-energy insertion of fig. 6.3 on the nucleon line, following the Dyson equation, hence substituting the particle nucleon propagator by a renormalized nucleon propagator including the nucleon self-energy in the medium,

$$G(p^0,\vec{p}) = \frac{1}{p^0 - \frac{\vec{p}^{\,2}}{2M_N} - \Sigma(p^0,\vec{p})} \tag{61}$$

where $\sum(p^0,\vec{p})$ is the nucleon self-energy. Alternatively one can use the spectral function representation [67]

$$G(p^0\vec{p}) = \int_{-\infty}^{\mu} d\omega \frac{S_h(\omega,\vec{p})}{p^0 - \omega - i\epsilon} + \int_{\mu}^{\infty} \frac{S_p(\omega,\vec{p})}{p^0 - \omega + i\epsilon} d\omega \tag{62}$$

where S_h, S_p are the hole and particle spectral functions related to Σ by means of [43]

$$\begin{aligned} &* \text{ If } \omega \geq \mu \quad , \quad S_p(\omega,p) = -\tfrac{1}{\pi} ImG(\omega,p) = -\tfrac{1}{\pi} \frac{Im\Sigma(\omega,p)}{A+B} \\ &* \text{ If } \omega \leq \mu \quad , \quad S_h(\omega,p) = \tfrac{1}{\pi} ImG(\omega,p) = \tfrac{1}{\pi} \frac{Im\Sigma(\omega,p)}{A+B} \end{aligned} \tag{63}$$

and μ is the chemical potential and

$$A = \left(\omega - \frac{\vec{p}^{\,2}}{2M_N} - Re\Sigma(\omega,\vec{p})\right)^2$$

$$B = \left(Im\Sigma(\omega,\vec{p})\right)^2$$

By means of eq.(62) we can write the ph propagator or new Lindhard function incorporating the effects of the nucleon self-energy in the medium and we have for $Im\bar{U}$

$$\begin{aligned} Im\,\bar{U}(q) = -\tfrac{1}{2\pi} \int_0^{\infty} dp\, p^2 \int_{-1}^{1} dx \int_{\mu-q^0}^{\mu} d\omega S_h(\omega,p) \times \\ \times S_p(q^0+\omega, \sqrt{\vec{p}^{\,2} + \vec{q}^{\,2} + 2pqx}) \end{aligned} \tag{64}$$

We use the spectral functions calculated in [42], but since the imaginary part of the nucleon self-energy for the hole states is much smaller than that of the particle states under consideration we make the approximation of setting to zero $Im\Sigma$ for the hole states. This was found to be a good approximation in [45]. Thus, we take

$$S_h(\omega,p) = \delta(\omega - \tilde{E}(\vec{p}))\Theta(\mu - \tilde{E}(p)) \tag{65}$$

where $\tilde{E}(p)$ is the energy associated to a momentum $\vec{p}$ obtained selfconsistently by means of the equation

$$\tilde{E}(\vec{p}) = \frac{\vec{p}^{\,2}}{2M_N} + Re\Sigma(\tilde{E}(\vec{p}),\vec{p}) \tag{66}$$

The chemical potential was then taken as

$$\mu = \frac{k_F^2}{2M_N} + Re\Sigma(\mu, k_F)$$

where k_F is the Fermi momentum.

It must be stressed that it is important to keep the real part of Σ in the hole states when renormalizing the particle states because there are pieces in the nucleon self-energy largely independent of the momentum and which cancel in the ph propagator, where the two selfenergies subtract.

The effect of the use of the spectral function, accounting for FSI is a quenching of the quasielastic peak and a spreading of the strength at higher energy as can be seen in fig. 6.4.

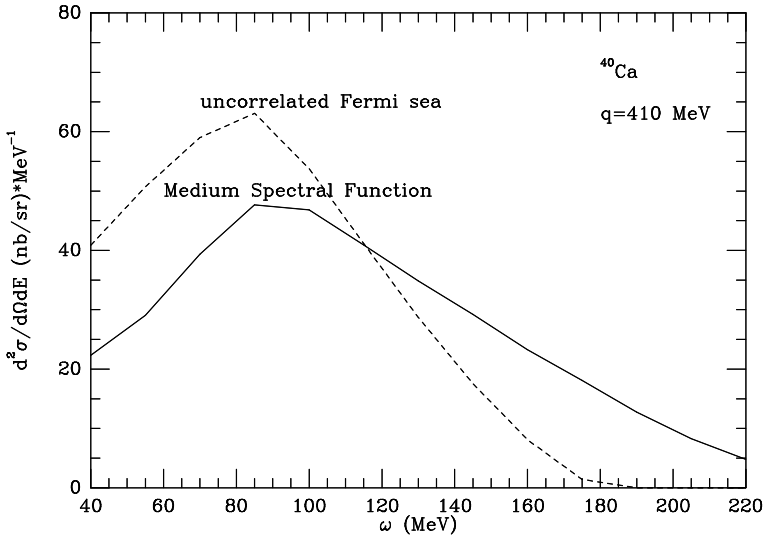

Fig.6.4 Effect of the use of the spectral function in the evaluation of the Lindhard function. The uncorrelated Fermi sea results are obtained from eqs.(57),(58). Those with the medium spectral function, with the same equations substituting the bare Lindhard function $\bar{U}$ by the medium modified one of eq.(64).

6.3 Polarization (RPA) effects in the quasielastic contribution

We take now into account polarization effects in the $1p1h$ excitation, substituting it by an RPA response as shown diagrammatically in fig. 6.5.

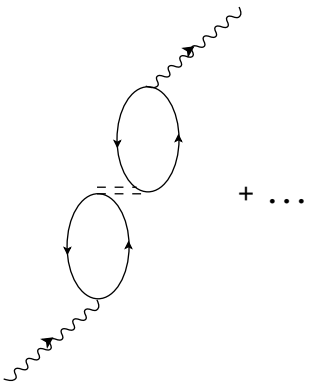

Fig.6.5 Diagrammatic representation of the polarization effects in the $1ph$ excitation.

For that purpose we use an effective interaction of the Landau-Migdal type

$$\begin{aligned} V(\vec{r}_1,\vec{r}_2) = \quad & c_0\delta(\vec{r}_1-\vec{r}_2)\left\{f_0(\rho)+f_0'(\rho)\vec{\tau}_1\vec{\tau}_2+\right. \\ & \left.+\,g_0(\rho)\vec{\sigma}_1\vec{\sigma}_2+g_0'(\rho)(\vec{\sigma}_1\vec{\sigma}_2)\vec{\tau}_1\vec{\tau}_2\right\} \end{aligned} \tag{67}$$

and we take the parameterization for the coefficients from ref. [68]

$$f_i(\rho(r)) = \frac{\rho(r)}{\rho(0)} f_i^{(in)} + \left[1-\frac{\rho(r)}{\rho(0)}\right] f_i^{(ex)} \tag{68}$$

$$\begin{aligned} & f_0^{(in)} = 0.07 && f_0'^{(ex)} = 0.45 \\ & f_0^{(ex)} = -2.15 && c_0 = 380\, MeV fm^3 \\ & f_0'^{(in)} = 0.33 && \\ & g_0^{(in)} = g_0^{(ex)} = g_0 = 0.575 && \\ & g_0'^{(in)} = g_0'^{(ex)} = g_0' = 0.725 && \end{aligned} \tag{69}$$

For consistency, in the $S=1=T$ channel ($\vec{\sigma}\vec{\sigma}\vec{\tau}\vec{\tau}$ operator) we have continued to use the interaction used in [32] which has been used for the renormalization of the pionic and pion related channels studied in the former sections. There is only a minor difference of about 4% in g_0' between the two parametrizations.

Recalling that we had

$$\Pi_{(1)}^{\mu\nu} = \frac{1}{2}\bar{U}_N(q)A_N^{\nu\mu}(q)e^2 \tag{70}$$

let us take the nonrelativistic reduction of $A^{\nu\mu}$ in order to see the effects of the RPA renormalizations

$$\begin{aligned} A^{\mu\nu} \equiv \quad & \sum_{r,r'}\chi_r\left[F_1^p(q)\delta^{\mu 0} - i\frac{\mu_p G_M(q)}{2M_N}(\vec{\sigma}\times\vec{q})_i\delta^{\mu i} + F_1^p\frac{(2\vec{p}+\vec{q})_i}{2M_N}\delta^{\mu i}\right]\chi_{r'}\times \\ & \times\chi_{r'}\left[F_1^p(q)\delta^{\nu 0} + F_1^p\frac{(2\vec{p}+\vec{q})_i}{2M_N}\delta^{\nu i} + i\frac{\mu_p G_M(q)}{2M_N}(\vec{\sigma}\times\vec{q})_i\delta^{\nu i}\right]\chi_r + \\ & +(p\leftrightarrow n) \end{aligned} \tag{71}$$

Given the spin-isospin structure, the electric and magnetic components will be renormalized in the following way:

a) Interaction $\vec{\sigma}\vec{\sigma}\vec{\tau}\vec{\tau}$: is the one we used to renormalize the pionic related channels in former sections. It affects only the magnetic components. If we write

$$\begin{aligned} A^{\mu\nu}_{mag.} = & \sum_{r,r'}\chi_r \left[-i\frac{\mu_p G_M(q)}{2M_N}(\vec{\sigma}\times\vec{q})_i\delta^{\mu i}\right]\chi_{r'}\times \\ & \times\chi_{r'}\left[i\frac{\mu_p G_M(q)}{2M_N}(\vec{\sigma}\times\vec{q})_i\delta^{\nu i}\right]\chi_r\frac{(1+\tau_3)}{2}+ \\ & +[\text{neutrons}]\frac{(1-\tau_3)}{2} \end{aligned} \tag{72}$$

it is easy to see that the magnetic part of Π^{ij} becomes

$$\begin{aligned} \Pi^{ij}_{mag.} = & \tfrac{1}{2}\bar{U}_N A^{ij}_{mag.}(q)e^2 + \frac{e^2}{4M_N^2}\frac{f^2_{\pi NN}}{m^2_\pi}\frac{V_t(q)}{1-\frac{f^2_{\pi NN}}{m^2_\pi}V_t(q)U(q)}\times \\ & \times(\vec{q}^{\,2}\delta^{ij}-q^iq^j)G^2_M(q)\left(\mu_p\bar{U}_p-\mu_n\bar{U}_n\right)^2 \end{aligned} \tag{73}$$

where $U = U_N + U_\Delta$.

b) Interaction $\vec{\tau}\vec{\tau}$:

This interaction selects the non magnetic components of V^μ. Thus A^{00} and the convective terms of A^{ij} (term with $2\vec{p}+\vec{q}$ in eq.(71)) are renormalized.

However, given the smallness of the convective terms (about 10% contribution to the transverse response) we shall not consider their renormalization.

Thus we consider only the modification to A^{00} from this source. Since A^{00} is given by

$$\begin{aligned} A^{00} = & \left[\sum_{r,r'}\chi_r F_1^p(q)\chi_{'}\chi_{r'}F_1^p(q)\chi_r\right]\frac{(1+\tau_3)}{2}+ \\ & +\left[\sum_{r,r'}\chi_r F_1^n(q)\chi_{r'}\chi_{r'}F_1^n(q)\chi_r\right]\frac{(1-\tau_3)}{2} \end{aligned} \tag{74}$$

the renormalized expression for Π^{00} will be

$$\Pi^{00} = e^2\left\{(F_1^p)^2\bar{U}_p + (F_1^n)^2\bar{U}_n + \frac{c_0 f_0'(F_1^p\bar{U}_p - F_1^n\bar{U}_n)^2}{1-c_0 f_0' U_N(q)}\right\} \tag{75}$$

where in the denominator we do not have now U_Δ since the operator $\vec{\tau}\vec{\tau}$ cannot excite Δ components.

c) Interaction $\vec{\sigma}\vec{\sigma}$:

Here again, like in case a), only the magnetic components are modified. We find

$$\Pi^{ij}_{mag.} = \frac{1}{2}\bar{U}_N A^{ij}_{mag.}(q)e^2 + \frac{e^2}{4M^2}c_0 g_0 \frac{1}{1 - c_0 g_0 U_N(q)} \times$$
$$\times(\vec{q}^{\,2}\delta^{ij} - q^i q^j) G_M^2(q) \left(\mu_p \bar{U}_p + \mu_n \bar{U}_n\right)^2 \qquad (76)$$
$$+ \; effect \; of \; (a)$$

The correction from the RPA sum is taken into account by means of the second term of the right hand side of eq.(76) to which we should add the same term in eq.(73) coming from the renormalization with the $\vec{\sigma}\vec{\sigma}\vec{\tau}\vec{\tau}$ operator.

d) Scalar interaction:

This one affects A^{00} and we find

$$\Pi^{00} = e^2 \left\{ (F_1^p)^2 \bar{U}_p + (F_1^n)^2 \bar{U}_n + \frac{c_0 f_0(\rho)(F_1^p \bar{U}_p + F_1^n \bar{U}_n)^2}{1 - c_0 f_0 U_N(q)} \right\} \; + \; effect \; of \; (b) \qquad (77)$$

We show in figs. 6.6, 6.7, 6.8 and 6.9 the effects on R_L and R_T ($R_L = -\frac{|\vec{q}|^2}{q^2} W_L$ and $R_T = 2W_T$) of the different polarization terms. The solid line corresponds to the calculation including these effects and the dashed line, to the calculation without polarization effects (we are using spectral functions in the calculation of the Lindhard function):

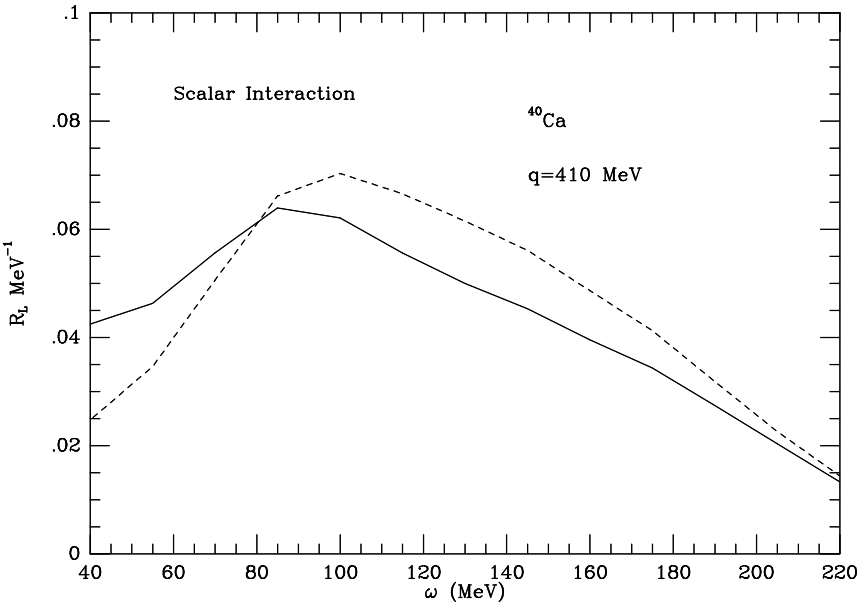

Fig.6.6 Polarization (RPA) effect (solid line) in the evaluation of R_L: scalar interaction.

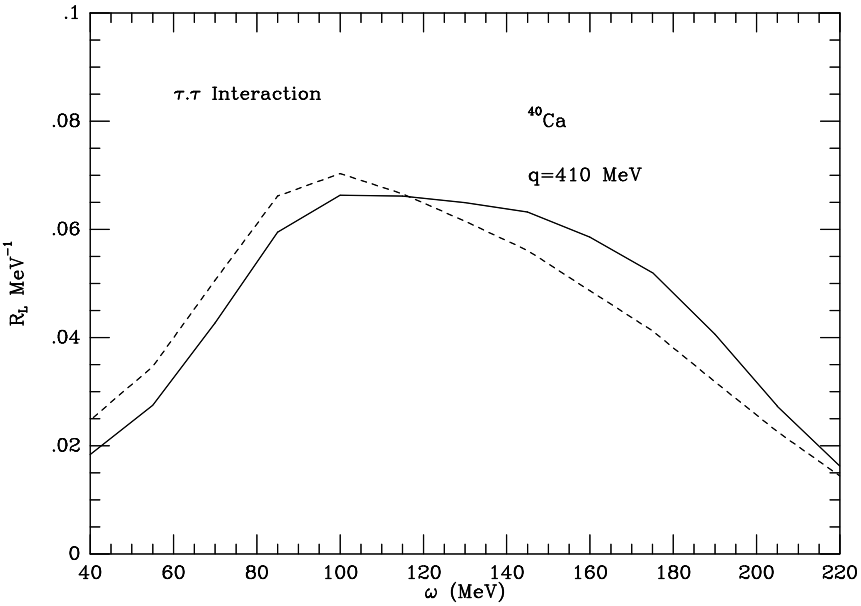

Fig.6.7 Polarization (RPA) effect (solid line) in the evaluation of R_L: $\vec{\tau}\vec{\tau}$ interaction.

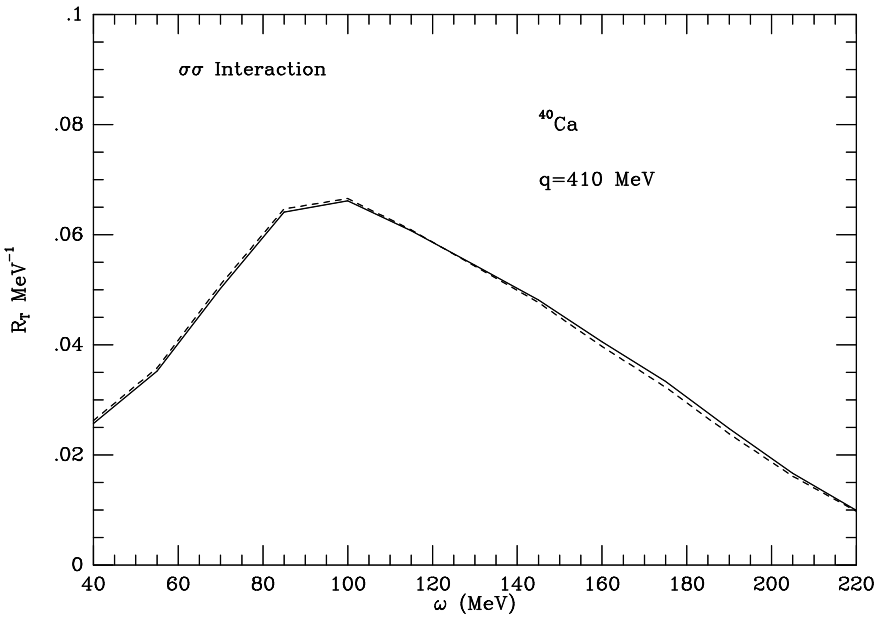

Fig.6.8 Polarization (RPA) effect (solid line) in the evaluation of R_T: $\vec{\sigma}\vec{\sigma}$ interaction.

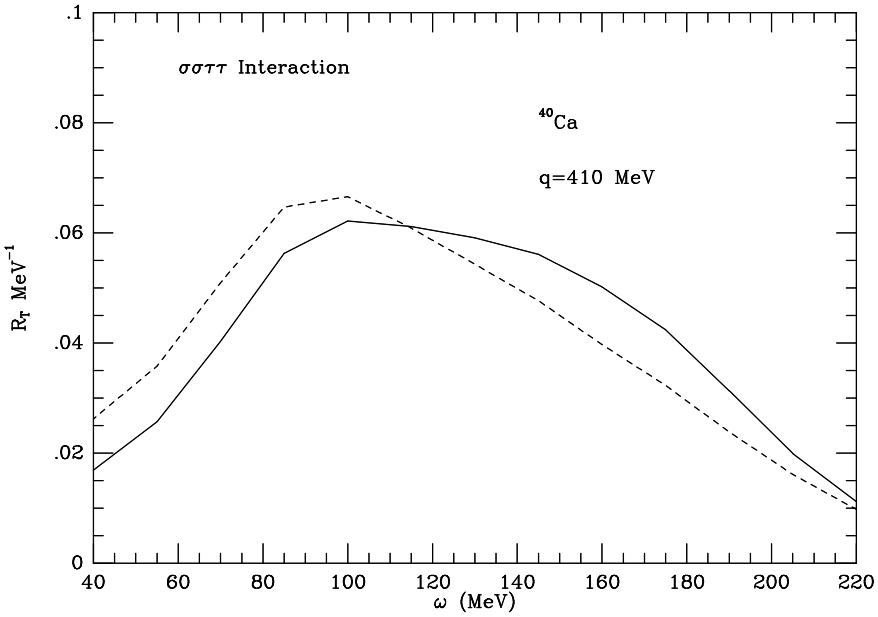

Fig.6.9 Polarization (RPA) effect (solid line) in the evaluation of R_T: $\vec{\sigma}\,\vec{\sigma}\,\vec{\tau}\,\vec{\tau}$ interaction.

One possible source of renormalization not yet considered is the one shown in fig. 6.10, where a ph is attached to one photon and a Δh to the other one, plus any other possible ph or Δh excitations in between.

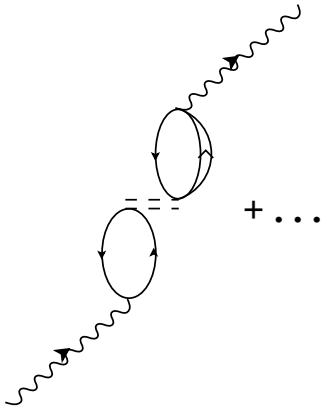

Fig.6.10 Diagrammatic representation of a possible source of renormalization: a ph is attached to one photon and a Δh to the other one, plus any other possible ph or Δh excitations in between.

This contribution affects the transverse part and both the quasielastic as well as the Δ peak. However, given the small interference between ph and Δh excitations, the contribution of these terms is not significant. We give, however, the expression here for completeness

$$\Pi^{ij} = e\left(\frac{4}{3}\right)^2 \frac{f_\gamma}{m_\pi} \frac{\rho}{\left(\sqrt{s} - M_\Delta + i\frac{\Gamma}{2} - \Sigma_\Delta\right)} i \times$$

$$\times \frac{V_t}{\left(1 - U\frac{f^2_{\pi NN}}{m^2_\pi} V_t\right)} \frac{f_{\pi NN}}{m_\pi} \frac{f^*}{m_\pi} [\vec{q}^{\,2}\delta^{ij} - q^i q^j] \times \tag{78}$$

$$\times \frac{G_M}{4M_N} [\mu_p \bar{U}_p - \mu_n \bar{U}_n]$$

The effect of the polarization is moderate, but relevant when aiming at a precise description of the process.

We show in figs. 6.11 and 6.12 the effects of the polarization in the longitudinal and transverse response functions. The net effect in the cross section is a quenching in the quasielastic peak and a spreading of the strength at higher energies.

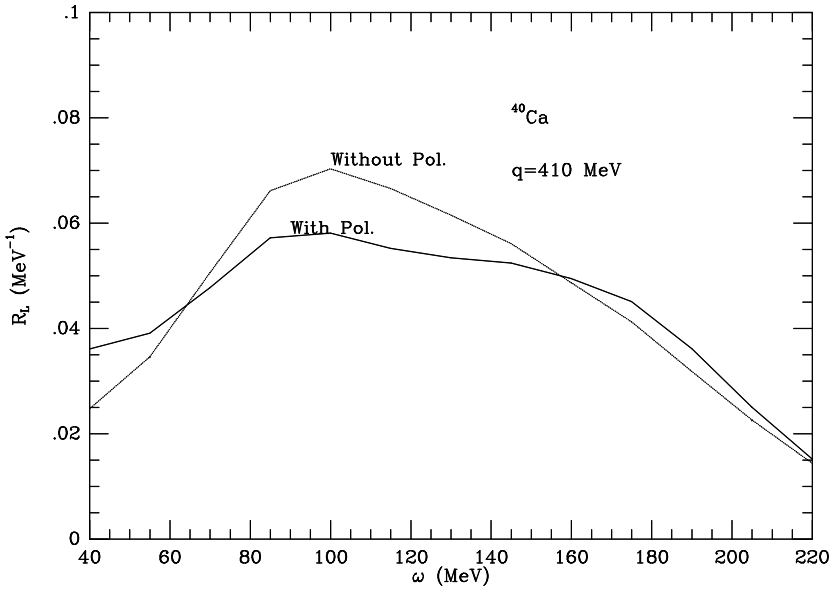

Fig.6.11 Polarization (RPA) effect in the evaluation of R_L.

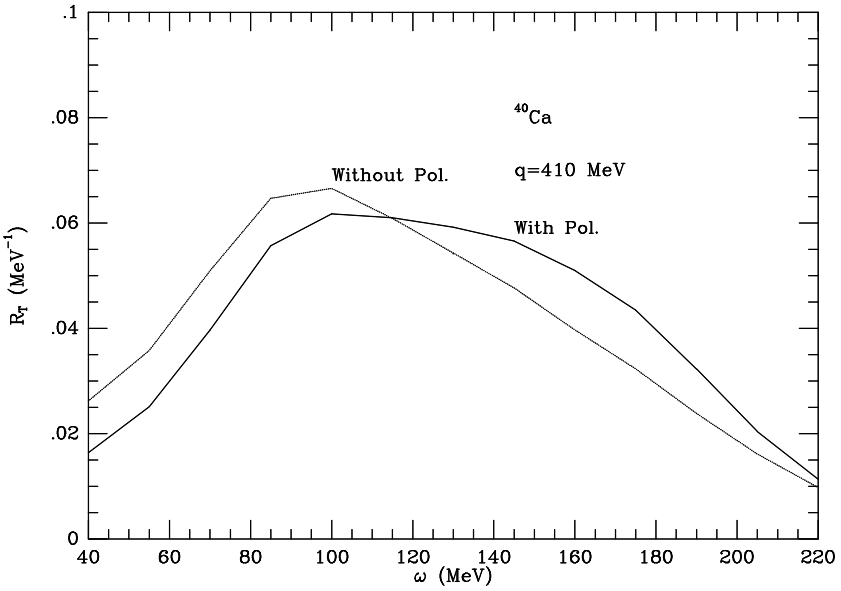

Fig.6.12 Polarization (RPA) effect in the evaluation of R_T.

6.4 Further considerations

Some other terms appearing in the generic diagram of fig. 4.11 require some special thought. These are the terms in which one of the vertices contains the nucleon pole term of the $\gamma^* N \to \pi N$ amplitude, while the other one contains all terms but that one. This is depicted in fig. 6.13.

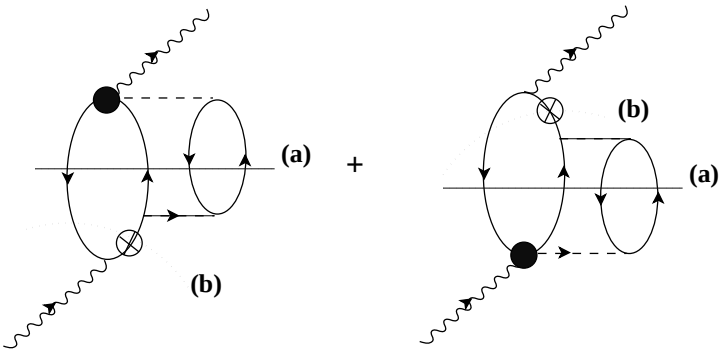

Fig.6.13 Photon self-energy diagrams in which one of the vertices contains the nucleon pole term of the $\gamma^* N \to \pi N$ amplitude, while the other one contains all terms but that one.

Unlike the case of real photons where only the cut (a) exciting $2p2h$ gives rise to an imaginary part, now the cut (b) placing the ph on shell is a source of imaginary part which produces strength is the quasielastic peak. The diagrams in fig. (6.13) for the cut (b) could be then considered an ordinary ph excitation with a renormalized vertex. We have evaluated the two sources of imaginary part in $\Pi^{\mu\nu}$ and find for the cut (a)

$$
\begin{aligned}
Im\Pi^{\mu\nu} = \; & \frac{f^2_{\pi NN}}{m^2_\pi}\sum_{ij}\int\frac{d^4p}{(2\pi)^4}n_i(\vec{p})(2\pi)\Theta(p^0)\delta\left(p^0 - E(\vec{p}) - Re\Sigma\left(\frac{\vec{p}^{\,2}}{2M_N},\vec{p}\right)\right)\times \\
& \times\int\frac{d^4k}{(2\pi)^4}F^4_\pi(k)\frac{\vec{k}^2_{CM}\Theta(k^0)}{(k^2-m^2_\pi)^2}2\pi\Theta(p^0+q^0-k^0)\times \\
& \delta\left(p^0+q^0-k^0 - E(\vec{p}+\vec{q}-\vec{k}\,) - Re\Sigma\left(\frac{(\vec{p}+\vec{q}-\vec{k}\,)^2}{2M_N},\vec{p}+\vec{q}-\vec{k}\right)\right)\times \\
& \times(1-n_j(\vec{p}+\vec{q}-\vec{k}\,))\frac{ImU_\lambda(k)}{1-\frac{f^2_{\pi NN}}{m^2_\pi}V_l(k)U(k)}(1-n_i(\vec{p}+\vec{q}))\times \\
& \times 2Re\left\{\frac{1}{p^0+q^0-E(\vec{p}+\vec{q})-\Sigma_N\left(\frac{(\vec{p}+\vec{q})^2}{2M_N},\vec{p}+\vec{q}\right)}\times\right. \\
& \left. Tr\left(\bar{\mathcal{M}}^{\mu}_{NP}(i\to j)\bar{\mathcal{M}}^{\dagger\nu}_{KR,PP,NPC,\Delta,\Delta C}(i\to j)\right)\right\}
\end{aligned}
\tag{79}
$$

where $\bar{\mathcal{M}}_{NP}$ is the nucleon pole amplitude of $\gamma^* N \to \pi N$ omitting the nucleon propagator. On the other hand the contribution of the cut (b) is given by

$$
\begin{aligned}
Im\Pi^{\mu\nu} = \; & -\sum_{ij}\int \frac{d^4p}{(2\pi)^4} n_i(p)\delta\left(p^0 - E(\vec{p}) - Re\Sigma\left(\frac{\vec{p}^{\,2}}{2M_N}, \vec{p}\right)\right)\times \\
& \times\Theta(p^0)(2\pi)^2(1-n_i(\vec{p}+\vec{q}))\Theta(p^0+q^0)\times \\
& \times\delta\left(p^0+q^0 - E(\vec{p}+\vec{q}) - Re\Sigma\left(\frac{(\vec{p}+\vec{q})^2}{2M_N}, \vec{p}+\vec{q}\right)\right)\times \\
& \int\frac{d^4k}{(2\pi)^4}F_\pi^2(k) Im\left\{\frac{(1-n_j(p+q-k))}{p^0+q^0-k^0-E(\vec{p}+\vec{q}-\vec{k}\,)+i\epsilon}\times\right. \\
& \times\left(\frac{1}{k^2-m_\pi^2-\Pi}-\frac{1}{k^2-m_\pi^2+i\epsilon}\right)\times \\
& \left.\times Tr\left(\bar{\mathcal{M}}^{\nu}_{KR,PP,NPC,\Delta,\Delta C}(i\to j)\bar{\mathcal{M}}^{\dagger\mu}_{NP}(i\to j)\right)\right\}
\end{aligned}
\tag{80}
$$

where Π is the pion self-energy in the nuclear medium

$$
\Pi = \vec{k}^2_{CM}\left(\frac{f_{\pi NN}}{m_\pi}\right)^2 F_\pi^2(k^2)\frac{U_\lambda(k)}{1-g'\left(\frac{f_{\pi NN}}{m_\pi}\right)^2 U(k)} \tag{81}
$$

the subtraction of the free pion propagator appearing in eq.(80) guarantees that in the limit $\rho \to 0$ the correction to the γNN vertex vanishes as it should be.

6.5 Considerations on gauge invariance

Most of the theoretical models found in the literature on inclusive (e, e') scattering from nuclei do not preserve gauge invariance. The requirement of invariance under gauge transformations leads to relations between the components (charge and spatial current) of the hadronic current which determines the nuclear response. Actually, the longitudinal (charge) multipoles are related to the two transverse (spatial current) multipoles of the electric type [80]. Several prescriptions have been used to restore gauge invariance [80], [81]. However, in a recent work [82] the arbitrariness of the most common prescriptions is discussed in detail with the conclusion that the standard procedures to impose gauge invariance in calculations, based on models which do not verify it, are misleading and for very low nuclear excitation energies do not ensure at all that a better, or a more reasonable, description of the data will be obtained.

Our model, as we shall see, is gauge invariant at the lowest order (impulse approximation) of the density expansion and this symmetry is only partially broken when some non-leading density corrections are included. In what follows, we will study the consequences of the partial breaking of the gauge symmetry for the kinematics studied in this paper (from the quasielastic peak to the Δ excitation region), which involves larger

nuclear excitation energies than those studied in [82]. We will also study the feasibility of non-gauge invariant models to disentangle between longitudinal and transverse channels.

The unpolarized cross section for inclusive (e, e') scattering from nuclei is given by (eq.(29)):

$$\frac{d^2\sigma}{d\Omega'_e dE'_e} = \frac{\alpha^2}{q^4}\frac{|\vec{k}'|}{|\vec{k}|}L^{\mu\nu}W_{\mu\nu} \tag{82}$$

Lorentz, space-inversion, time-reversal and gauge invariance constraint the form of the hadronic tensor $W_{\mu\nu}$, which determines the nuclear response. Indeed, the most general expression for this tensor assuming the latter symmetries is given by [83]:

$$\begin{aligned} W^{\mu\nu} &= \{\frac{q^\mu q^\nu}{q^2} - g^{\mu\nu}\}W_1 \\ &+ \left\{\left(P^\mu - \frac{P.q}{q^2}q^\mu\right)\left(P^\nu - \frac{P.q}{q^2}q^\nu\right)\frac{W_2}{M_A^2}\right\} \end{aligned} \tag{83}$$

with q and P the virtual photon and initial hadronic system four-momenta respectively and $M_A^2 = P^2$. The structure functions $W_{1,2}$ are unknown scalar functions of the virtual photon variables which determine the nuclear response.

Using the expression for the hadronic tensor of eq. (83) and taking $\vec{q}$ in the z direction the cross section of eq. (82) in the lab system becomes (eq. (31)):

$$\frac{d^2\sigma}{d\Omega'_e dE'_e} = \left(\frac{d\sigma}{d\Omega}\right)_{Mott}\left(-\frac{q^2}{|\vec{q}|^2}\right)\left\{W_L(\omega, |\vec{q}|) + \frac{W_T(\omega, |\vec{q}|)}{\epsilon}\right\} \tag{84}$$

where the structure functions W_L and W_T are given in terms of W_1 and W_2 by:

$$W_L \equiv -W_1 - \frac{|\vec{q}|^2}{q^2}W_2 = -\frac{q^2}{\omega^2}W^{zz} = -\frac{q^2}{|\vec{q}|^2}W^{00} = -\frac{q^2}{\omega|\vec{q}|}W^{0z} \tag{85}$$

$$W_T \equiv W_1 = W^{xx} = W^{yy} \tag{86}$$

Let us now suppose that the hadronic model does not preserve gauge invariance. In these circumstances the hadronic tensor (we will call it $\mathcal{W}^{\mu\nu}$ to differentiate it from the one defined in eq. (83)) is not conserved (ie, $q_\mu\mathcal{W}^{\mu\nu} \neq 0$, $q_\nu\mathcal{W}^{\mu\nu} \neq 0$), and is now given in terms of four independent functions:

$$\begin{aligned} \mathcal{W}^{\mu\nu} &= \{\frac{q^\mu q^\nu}{q^2} - g^{\mu\nu}\}W_1 \\ &+ \left\{\left(P^\mu - \frac{P.q}{q^2}q^\mu\right)\left(P^\nu - \frac{P.q}{q^2}q^\nu\right)\frac{W_2}{M_A^2}\right\} \\ &+ W_3\frac{q^\mu q^\nu}{q^2} + W_4\frac{P^\mu P^\nu}{M_A^2} \end{aligned} \tag{87}$$

Because of the loss of gauge invariance now $\mathcal{W}^{00}$, $\mathcal{W}^{0z}$ and $\mathcal{W}^{zz}$ are no longer related and become independent. Thus, we have now:

$$W_L \equiv -W_1 - \frac{|\vec{q}|^2}{q^2} W_2 = \frac{|\vec{q}|}{\omega}\mathcal{W}^{0z} - \mathcal{W}^{zz} \tag{88}$$

$$W_T \equiv W_1 = \mathcal{W}^{xx} = \mathcal{W}^{yy} \tag{89}$$

$$W_3 = \frac{\omega}{|\vec{q}|}\mathcal{W}^{0z} - \mathcal{W}^{zz} \tag{90}$$

$$W_4 = \mathcal{W}^{00} + \mathcal{W}^{zz} - \left(\frac{|\vec{q}|}{\omega} + \frac{\omega}{|\vec{q}|}\right)\mathcal{W}^{0z} \tag{91}$$

If gauge invariance is restored and therefore the hadronic tensor is conserved, the response functions W_3 and W_4 vanish and W_L reduces to any of the expressions of eq. (85). With this new hadronic tensor the differential cross section is now given by:

$$\frac{d^2\sigma}{d\Omega'_e dE'_e} = \left(\frac{d\sigma}{d\Omega}\right)_{Mott}\left(-\frac{q^2}{|\vec{q}|^2}\right)\left\{\mathcal{W}_L(\omega,|\vec{q}|) + \frac{W_T(\omega,|\vec{q}|)}{\epsilon}\right\} \tag{92}$$

with

$$\begin{aligned}\mathcal{W}_L(\omega,|\vec{q}|) &= \left(W_L(\omega,|\vec{q}|) - \frac{|\vec{q}|^2}{q^2}W_4(\omega,|\vec{q}|)\right) \\ &= -\frac{\omega^2}{q^2}\mathcal{W}^{zz} - \frac{|\vec{q}|^2}{q^2}\mathcal{W}^{00} + 2\frac{|\vec{q}|\omega}{q^2}\mathcal{W}^{0z}\end{aligned} \tag{93}$$

The function W_3 does not appear in the expression for the cross section because the leptonic tensor is conserved. Note that, one can still factor out the differential cross section in the form $A + B/\epsilon$ and therefore, despite the breaking of gauge invariance, one can still compare the results to the experimental response functions obtained via the Rosenbluth plot. Then, the breaking of gauge invariance in the theoretical model for the nuclear response leads to a redefinition of the response function which has to be compared to the experimental one, in the longitudinal channel, and thus one should compute $\mathcal{W}_L$ given in eq. (93) instead of W_L of eq. (85). In fact, the latter one is not well defined and there is an arbitrariness in its definition because the 00, $0z$ and zz components of $\mathcal{W}^{\mu\nu}$ are no longer related.

Traditionally, the longitudinal response function is calculated from the "charge-charge" component of the hadronic tensor ($-q^2/|\vec{q}|^2\mathcal{W}^{00}$). In general, the response function calculated in this way will differ from that calculated by means of eq. (93). Now we will examine the difference between both approaches as a function of the energy and momentum transferred to the nucleus. In order to do that, we define

$$\mathcal{W}^{zz} = \frac{\omega^2}{|\vec{q}|^2}\mathcal{W}^{00} + \Delta\mathcal{W}^{zz} \tag{94}$$

$$\mathcal{W}^{0z} = \frac{\omega}{|\vec{q}|}\mathcal{W}^{00} + \Delta\mathcal{W}^{0z} \tag{95}$$

where $\Delta\mathcal{W}^{zz}$ and $\Delta\mathcal{W}^{0z}$ account for the breaking of the gauge symmetry. By construction one expects:

$$\frac{\Delta\mathcal{W}^{zz}}{\mathcal{W}^{00}} \approx \delta_1 \frac{\omega^2}{|\vec{q}|^2} \tag{96}$$

$$\frac{\Delta\mathcal{W}^{0z}}{\mathcal{W}^{00}} \approx \delta_2 \frac{\omega}{|\vec{q}|} \tag{97}$$

where δ_1 and δ_2 would be 1 in the case that $\Delta\mathcal{W}^{zz} = \mathcal{W}^{zz}$ and $\Delta\mathcal{W}^{0z} = \mathcal{W}^{0z}$. We certainly expect that in our case δ_1 and δ_2 are smaller than 1 because at order ρ in the density expansion we exactly fulfill gauge invariance (see comments below). Taking a conservative point of view one sees that the ratios in eqs. (96), (97) are at most of order 1. Using the definitions of eq. (94), we can now write

$$\mathcal{W}_L = -\frac{q^2}{|\vec{q}|^2}\mathcal{W}^{00}\left\{1 + \frac{\omega^2|\vec{q}|^2}{q^4}\frac{\Delta\mathcal{W}^{zz}}{\mathcal{W}^{00}} - 2\frac{\omega|\vec{q}|^3}{q^4}\frac{\Delta\mathcal{W}^{0z}}{\mathcal{W}^{00}}\right\} \tag{98}$$

The size of the corrections to the "charge-charge" prescription (the term proportional to 1 in the formula) traditionally used in the literature depends on the kinematics under study. Here we will pay a special attention to three different regions (keeping always the momentum transferred to the nucleus smaller than about 500 MeV) : Δ-resonance and quasielastic peaks and the region (*dip*) between both peaks.

- Quasielastic peak: In this region we have $\omega \approx |\vec{q}|^2/2M_N$ and then the coefficients of the ratios $\frac{\Delta\mathcal{W}^{zz}}{\mathcal{W}^{00}}$ and $\frac{\Delta\mathcal{W}^{0z}}{\mathcal{W}^{00}}$ in eq. (96) turn out to be

$$\frac{\omega^2|\vec{q}|^2}{q^4} \approx \frac{|\vec{q}|^2}{4M_N^2} \tag{99}$$

$$2\frac{\omega|\vec{q}|^3}{q^4} \approx \frac{|\vec{q}|}{M_N} \tag{100}$$

  Thus, taking also into account the estimates of eq. (96), one finds corrections to the "charge-charge" prescription of the order of $\delta_2|\vec{q}|^2/2M_N^2$ which at most could be of the order of $5-10\%$ for the momenta and energies transfers studied in this paper, assuming $\delta_2 \approx 1$, which is certainly an overestimate for the reasons pointed above. From this discussion, in this region we have decided to use the traditional prescription "charge-charge" to compute the longitudinal response function.

- *Dip* area: In this region the conclusions are similar to those drawn in the previous point. However, we would like to point out that gauge symmetry breaking corrections to the longitudinal response function are not now as small as before.

- Δ-resonance peak: In this region $\omega/|\vec{q}| \approx 1$ and the situation is radically different. The corrections due to gauge symmetry breaking are significantly more important than in the quasi-free scattering region. For instance, taking the incoming electron energy equal to 620 MeV and the outgoing electron scattering

angle equal to 60^0, one finds values for the coefficients of the ratios $\frac{\Delta\mathcal{W}^{zz}}{\mathcal{W}^{00}}$ and $\frac{\Delta\mathcal{W}^{0z}}{\mathcal{W}^{00}}$ in eq. (98) of the order of two. Thus the corrections to unity in the bracket of eq. (98), are of the order of $2(\delta_1 - \delta_2)$, much larger than in the quasielastic peak. We have evaluated δ_1 and δ_2 in this region and we find $\delta_1 \approx 0.01 - 0.06$, $\delta_2 \approx 0.01 - 0.02$ and $2(\delta_1 - \delta_2) \approx 0.0 - 0.08$. Hence a 10% error in the longitudinal response due to the breaking of gauge invariance of our results seems realistic in this region. In any case, we should mention that the contribution of the longitudinal response to the cross section is very small here and hence theoretical cross sections are largely free of uncertainties due to the small breaking of gauge invariance. Since there is no experimental separation of R_L and R_T in this region, we do not give these results either.

We finish this section discussing the origin of the breaking of the gauge invariance within our model. Let us consider the diagram of fig. 6.1 whose contribution to the virtual photon self-energy in the medium is given in eqs.(53) and (54). One can easily check that the imaginary part (when the intermediate nucleons are put on shell) of this self-energy is gauge invariant ($q_\mu \Pi^{\mu\nu} \propto q_\mu V^\mu = 0$). The first medium correction is given by the diagram depicted in fig.6.2. When the two ph excitations are put on shell, this diagram contributes to the imaginary part of the photon self-energy. This new contribution is not gauge invariant because the intermediate nucleon with four momentum $p + q$ is not on shell and then the contraction $q_\mu V^\mu$ does not vanish now. However, to this level we restore gauge invariance because we consider not only the term of fig. 6.2, but also all terms implicit in fig. 4.9. Though the NP amplitude in not gauge invariance by itself, the thick dots of fig. 4.9 account for the six amplitudes (NP+NPC+KR+PP+DP+DPC) of our model for the $eN \to e'N\pi$ reaction. In section 3, we fixed the different form-factors entering in the amplitudes to end up with a gauge invariant model (Eqs.(8-9)). Thus, the leading terms in our density expansion (fig.6.1, fig. 4.2 and fig. 4.9) lead to a gauge invariant photon self-energy.

However, we break again the gauge invariance in section 4.7 when we include the polarization corrections to the 36 diagrams of fig. 4.9: we do not renormalize in the same way for instance the $KR \times KR$ term (which is purely longitudinal and therefore gets renormalized only with V_l) than the $NP \times NP$ term (which contributes to both longitudinal and transverse channels and thus gets renormalized not only with V_l but also with V_t). As a consequence, the cancellations in eq.(8) which ensured the gauge invariance of the model are altered.

7 Results

We have already shown results on the different effects in previous sections. Here we will show results with emphasis in comparison with experiment.

Let us first show results in the quasielastic peak in figs. 7.1, 7.2 we show results for R_L and R_T for ^{12}C and compare them to the data of [70]. The lower line shows the results obtained with the medium spectral function, while the upper one includes also the rest of the effects discussed in the former section.

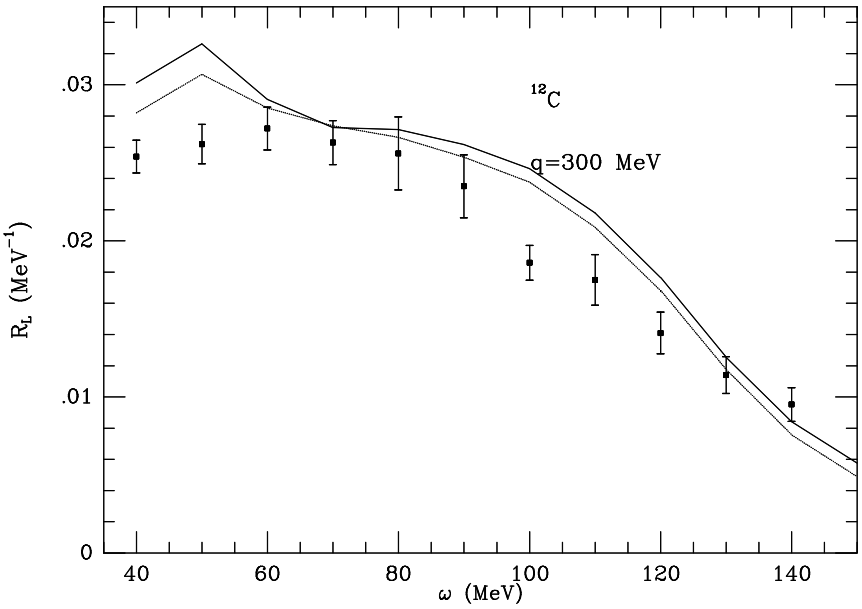

Fig.7.1 Calculation of R_L for ^{12}C. The lower line in the high energy region corresponds to the result obtained with the contribution of the $1p1h$ excitation (fig. 6.3) using the medium spectral function of eq.(64). The upper line is the result when one adds the rest of contributions: vertex corrections (fig. 6.13), two body absorption diagrams (fig. 4.9), (γ^*, π) terms (fig. 4.2), $(\gamma^*, 2\pi)$ related terms (fig. 4.15), etc. Experimental data from [70].

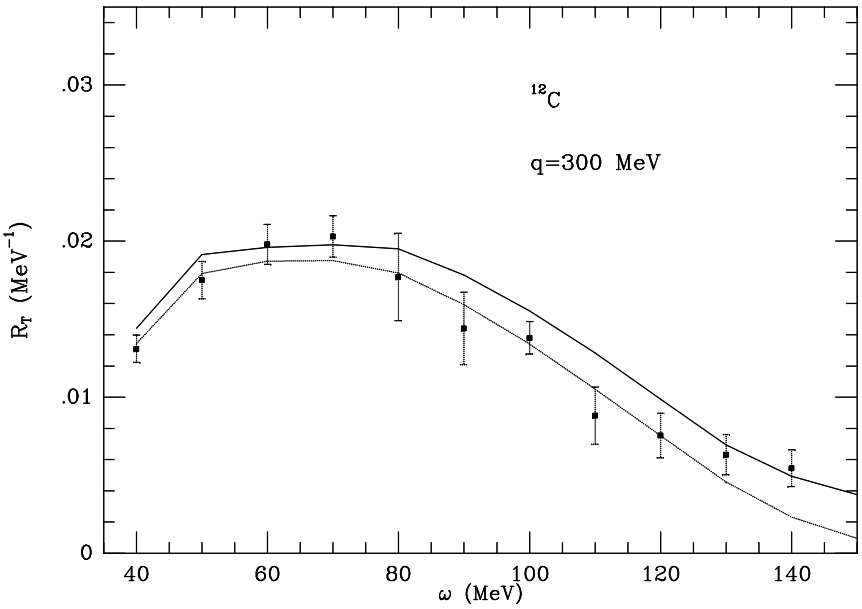

Fig.7.2 Calculation of R_T for ^{12}C. Same meaning of the lines as in fig. 7.1. Experimental data from [70].

In fig. 7.3, 7.4, we show results for ^{40}Ca compared to the data of [7] (fig. (7.3) and lower points in fig. (7.4)) and those of [1] (upper points in fig. (7.4)).

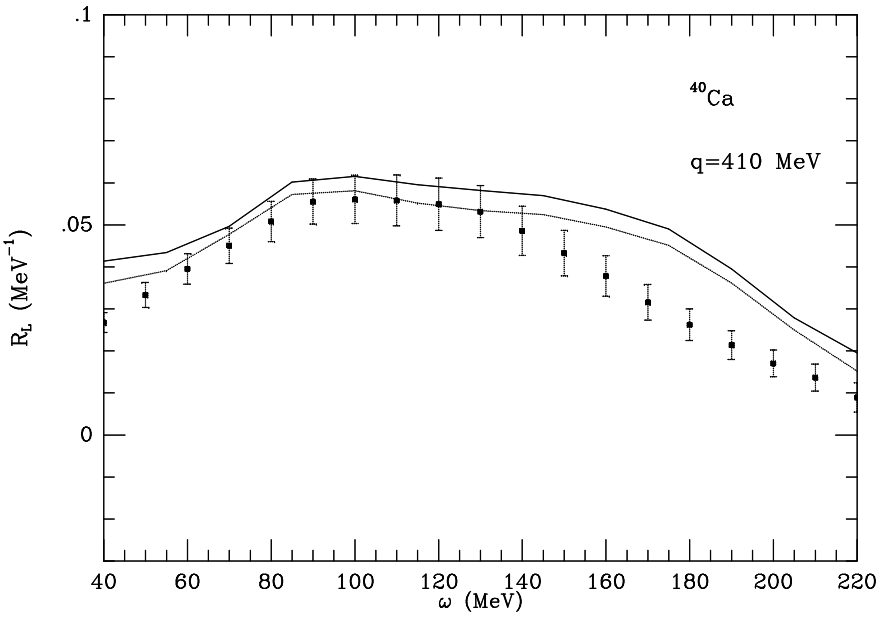

Fig.7.3 Calculation of R_L for ^{40}Ca. Same meaning of the lines as in fig. 7.1. Experimental data from [7].

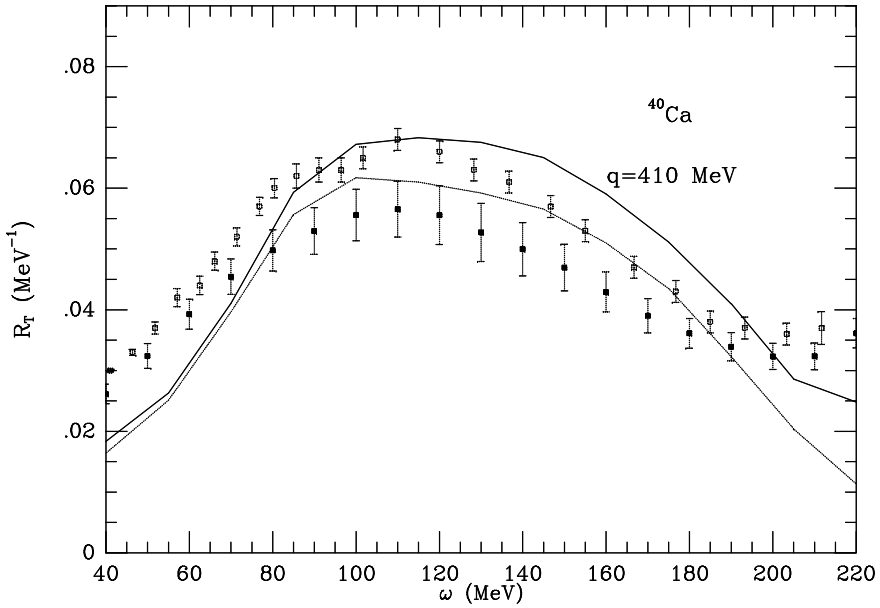

Fig.7.4 Calculation of R_T for ^{40}Ca. Same meaning of the lines as in fig. 7.1. Experimental data from [7] (lower points) and [1] (upper points).

As one can see, we find a good agreement with the recent reanalysis of [7].

On the other hand much of the work done here has gone into the evaluation of two body mechanisms. In fig. 7.5 we show the results for two body photon absorption (solid line) and compare them to pion production (dotted line). Similarly, in fig. 7.6 we show the contribution of three body photon absorption (solid line) versus the two body one (dotted line). We can see that at low energies, the contribution of three body

absorption is negligible while at energies around 450 MeV the three body contribution becomes sizeable. These results agree qualitatively with the findings of [84] for real photons. Let us recall that this classification corresponds to the primary step in the collision. The particles produced still undergo secondary collisions in their way out of the nucleus. This does not change the inclusive cross section but redistributes the strength. The treatment of this FSI and the evaluation of the exclusive channels will be treated in a forthcoming paper [57].

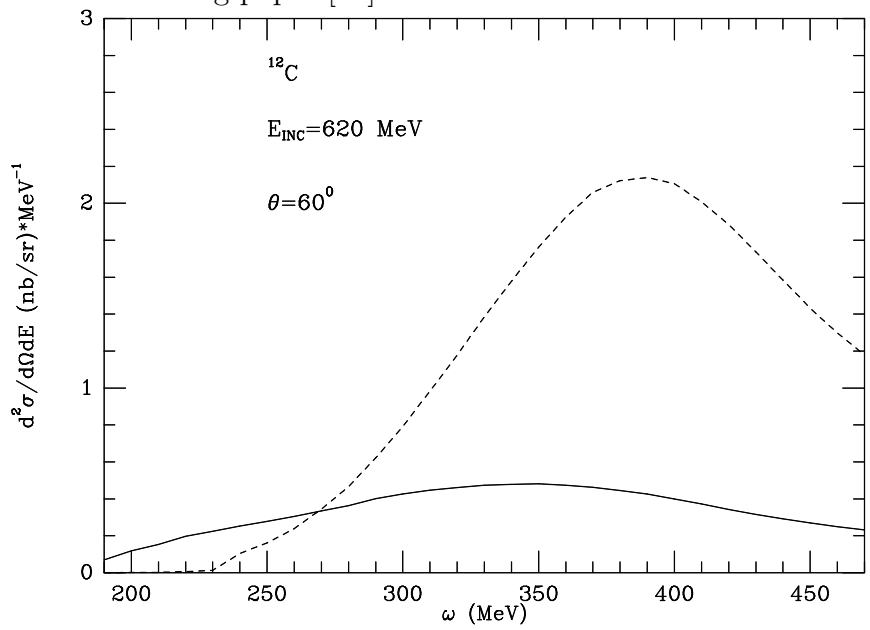

Fig.7.5 Two body photon absorption (solid line) versus pion production (dotted line) for ^{12}C.

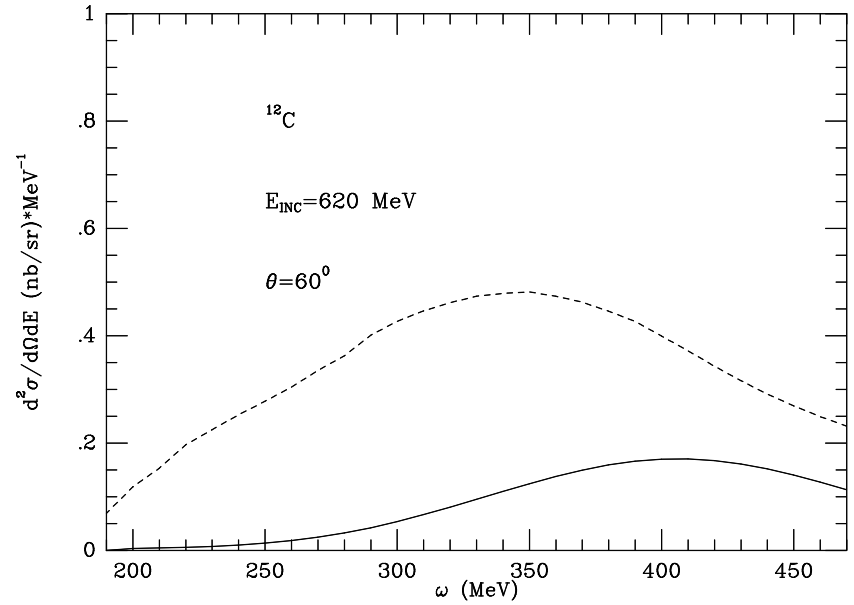

Fig.7.6 Three body photon absorption (solid line) versus the two body one (dotted line) for ^{12}C.

Finally let us see the global results including the quasielastic peak, the dip region and the delta region. They can be seen in figs. 7.7, 7.8 and 7.9 for the nuclei of ^{12}C and ^{208}Pb.

The global agreement is good and the three regions are well reproduced (a bit overestimated for ^{208}Pb).

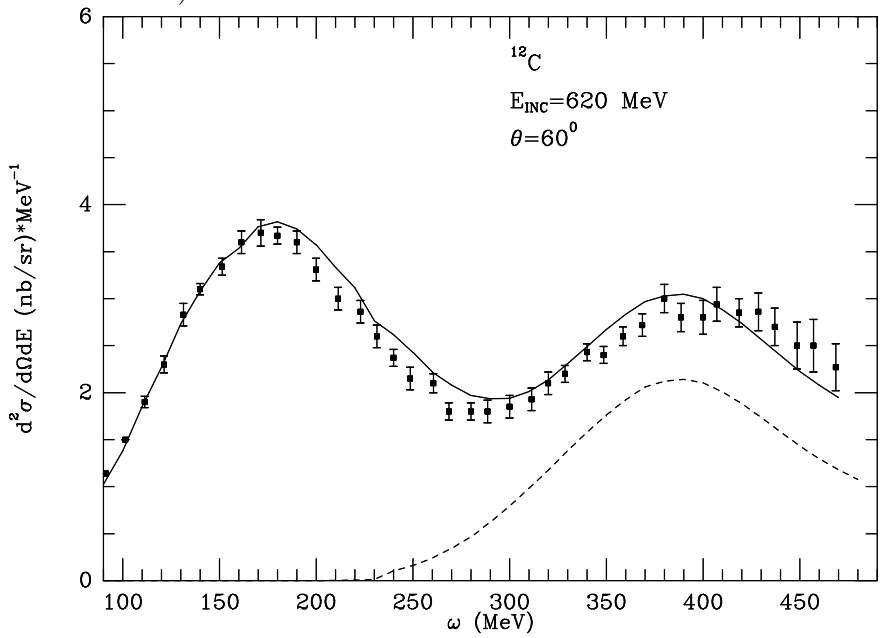

Fig.7.7 Inclusive (e, e') cross section for ^{12}C. $E_e = 620$ MeV and $\theta_e = 60^0$. The dotted line corresponds to the pion production contribution. Experimental data from [3].

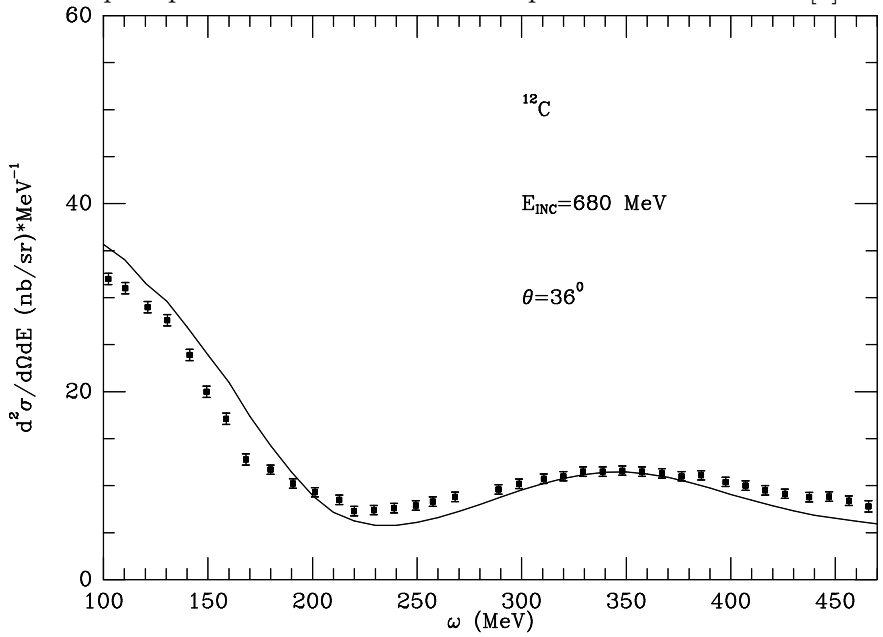

Fig.7.8 Inclusive (e, e') cross section for ^{12}C. $E_e = 680$ MeV and $\theta_e = 36^0$. Experimental

data from [3].

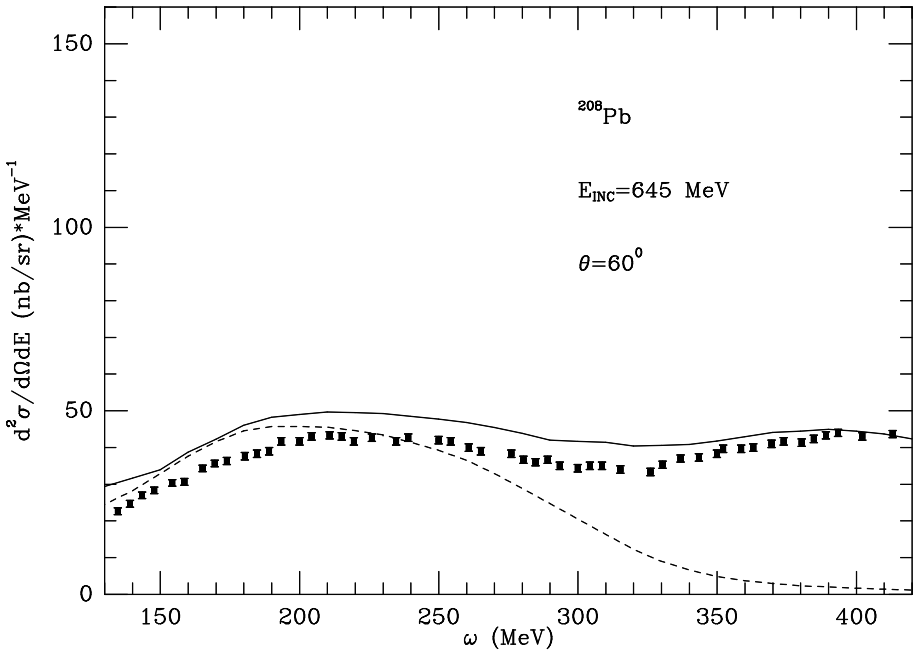

Fig.7.9 Inclusive (e, e') cross section for ^{208}Pb. $E_e = 645$ MeV and $\theta_e = 60^0$. The dotted line corresponds to the $1p1h$ excitation contribution. Experimental data from [73].

In fig. 7.7 we also show with a dotted line the results for pion production.

In fig. 7.9 instead we show with a dotted line the results for the $1p1h$ excitation alone.

8 Conclusions

We have undertaken the task of constructing a microscopic many body model of the (e, e') reaction including all the reaction channels which appear below $\omega = 500 - 600$ MeV, and which is suited to study the inclusive (e, e') reaction from the quasielastic peak up to the Δ peak, passing through the dip region. Although many studies have been devoted to particular energy regions of the spectrum, this is the first work, to our knowledge, which ranges this wide energy spectrum.

Our model has no free parameters. All the input consists of basic couplings of photons to nucleons and isobars, and some phenomenological inputs, as correlations, which has been tested in former pionic reactions.

We include explicitly the $1N$ knockout channel, the virtual photon absorption by pairs or trios of particles, the pion production plus exchange currents mechanisms tied to the $(\gamma^*, 2\pi)$ channel and which contribute to $(\gamma^*, NN\pi)$ or (γ^*, NNN) channels.

We include effects which have been found important in earlier works, like polarization, renormalization of Δ properties in a nuclear medium, FSI effects through the use of spectral functions and meson exchange currents.

The meson exchange currents are generated in a systematic way from a model for the elementary pion electroproduction on the nucleon, which reproduces accurately the

experimental data.

We have payed some attention to the question of gauge invariance, showing that it is preserved in our approach in leading order of the density expansion. We also show that the appropriate prescription to evaluate the longitudinal response is from the W^{00} component of the hadronic tensor, which minimizes the breaking of gauge invariance at higher orders in ρ.

We evaluate cross sections in the energy range from the quasielastic peak to the Δ peak and find good agreement with experimental data. The three traditional regions: quasielastic peak, dip region and delta peak, are well reproduced in our scheme.

We also separate the longitudinal and transverse response functions in the quasielastic peak and find good agreement with the latest results of the analysis of Jourdan from the world set of data.

We have used the technique of the local density approximation, which has been shown before to be particularly suited to deal with inclusive cross sections and which makes unnecessary the use of sophisticated finite nuclei wave functions.

Finally, the method used here allows the separation of the contribution of different channels to the inclusive cross section. This information is the seed to produce exclusive cross sections like $(e, e'N)$, $(e, e'NN)$, $(e, e'\pi)$, $(e, e'\pi N)$ etc. However, this still requires to follow the fate of all the particles produced from their production point in the nucleus, which is usually done using Monte Carlo simulation techniques, and this will be the subject of some future work.

We would like to acknowledge useful discussions with R.C. Carrasco, C. García-Recio and A. Lallena. This paper is partially supported by CICYT contract no. AEN 96-1719. One of us (J. Nieves) thanks to DGES contract PB95-1204.

Appendix

The Galilean invariant vertices which appear in the model for $eN \to e\pi N$, are:

(a) γNN vertex (fig. 3.1(a)):

$$V^{\mu}_{\gamma NN} = -ie \left\{ \begin{array}{c} F_1^N(q^2) \\ \\ F_1^N(q^2) \left[\frac{\vec{p}+\vec{p}'}{2M_N} \right] + i \frac{\vec{\sigma} \times \vec{q}}{2M_N} G_M^N(q^2) \end{array} \right\} \tag{101}$$

(b) $\gamma N\Delta$ vertex (fig. 3.1(c)):

$$V^{\mu}_{\gamma N\Delta} = \sqrt{\frac{2}{3}} \frac{f_\gamma(q^2)}{m_\pi} \frac{\sqrt{s}}{M_\Delta} \left\{ \begin{array}{c} \frac{\vec{p}_\Delta}{\sqrt{s}} (\vec{S}^\dagger \times \vec{q}) \\ \\ \frac{p^0_\Delta}{\sqrt{s}} \left\{ \vec{S}^\dagger \times \left(\vec{q} - \frac{q^0}{p^0_\Delta} \vec{p}_\Delta \right) \right\} \end{array} \right\} \tag{102}$$

(c) $\pi N\Delta$ vertex (fig. 3.1(d)):

$$V_{\pi N\Delta} = I \frac{f^*}{m_\pi} \vec{S}^\dagger . \left(\vec{k} - \frac{k^0}{\sqrt{s}} \vec{p}_\Delta \right) \tag{103}$$

(d) πNN vertex (fig. 3.1(b)):

$$V_{\pi NN} = \frac{f_{\pi NN}}{m_\pi} B(N, N'\pi) \left\{ \vec{\sigma}\, \vec{k} - \frac{k^0}{2M_N} \vec{\sigma}\, (\vec{p} + \vec{p}') \right\} \tag{104}$$

where $\vec{q}$, $\vec{p}$, $\vec{p}'$, $\vec{p}_\Delta$ y $\vec{k}$ are the photon, incoming nucleon, outgoing nucleon and pion momenta, respectively; $\sqrt{s}$, the invariant energy in the $\gamma^* N$ system and M_N, m_π and M_Δ are the nucleon, pion and delta resonance masses. In equations (103) and (104) we are including the corresponding isospin factors I y $B(N, N'\pi)$, respectively.

Besides the vertices shown in fig. 3.1, in our elementary model for electroproduction two more vertices appear:

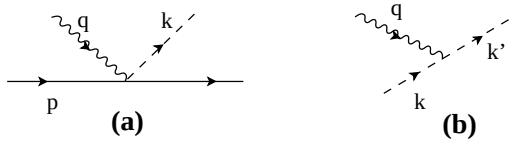

Fig. A.1

In fig. A.1(a) one can see the seagull vertex. It appears from the $\mathcal{L}_{\pi NN}$ lagrangian via minimal coupling. This vertex is exactly zero for the $\pi^0 n$ and $\pi^0 p$ channels and has the following expression:

$$V^{\mu}_{seagull} = e \frac{f_{\pi NN}}{m_\pi} B(N, N'\pi) F_A C^{\mu} \tag{105}$$

where

$$C^{\mu}(\pi^{-}p) = \begin{pmatrix} \dfrac{\vec{\sigma}\,(2\vec{p}\,+\,\vec{q}\,-\,\vec{k})}{2M_N} \\ \\ \vec{\sigma} \end{pmatrix} \quad ; \quad C^{\mu}(\pi^{0}n) = 0$$

$$C^{\mu}(\pi^{+}n) = \begin{pmatrix} \dfrac{\vec{\sigma}(\vec{k}\,-\,\vec{q}\,-\,2\vec{p})}{2M_N} \\ \\ \vec{\sigma} \end{pmatrix} \quad ; \quad C^{\mu}(\pi^{0}p) = 0$$

In figure A.1, the vertex (b) corresponds to the $\pi\pi\gamma^{*}$ coupling and it is defined as:

$$V^{\mu}_{\pi\pi\gamma^{*}} = ie(k^{\mu}\,+\,k'^{\mu}) \tag{106}$$

With respect to form factors and coupling constants, their expressions are the following:

We use Sachs Form Factors:

$$G^{N}_{M}(q^2) = \frac{\mu_N}{\left(1-\dfrac{q^2}{\Lambda^2}\right)^2} \quad ; \quad G^{N}_{E}(q^2) = \frac{1}{\left(1-\dfrac{q^2}{\Lambda^2}\right)^2} \tag{107}$$

with $\Lambda^2 = 0.71\ GeV^2$; $\mu_p = 2.793$; $\mu_n = -1.913$. The relationship between $F^{p}_{1}(q^2)$ (Dirac form factor) and G^{p}_{E} is:

$$F^{p}_{1}(q^2) = G^{p}_{E}\frac{\left(1-\dfrac{q^2}{4{M_N}^2}\mu_p\right)}{\left(1-\dfrac{q^2}{4{M_N}^2}\right)} \tag{108}$$

and $F^{n}_{1} = 0$.

For the rest of form factors and coupling constants we take:

$$\frac{f^2_{\pi NN}}{4\pi} \,=\, 0.08\ ; \quad \frac{f^{*2}}{4\pi} \,=\, 0.36\ ; \quad F_A(q^2) = \frac{1}{\left(1-\dfrac{q^2}{{M_A}^2}\right)^2} \tag{109}$$

where $M_A = 1.08\,GeV$.

$$F_{\gamma\pi\pi}(q^2) = \frac{1}{\left(1-\dfrac{q^2}{p^2_\pi}\right)} \tag{110}$$

with $p^2_\pi = 0.47\,GeV^2$.

$$F_\pi(q^2) = \frac{\Lambda^2_\pi - m^2_\pi}{\Lambda^2_\pi - q^2} \quad ; \quad \Lambda_\pi \sim 1250\,MeV \tag{111}$$

$$f_\gamma(q^2) = f_\gamma(0)\frac{\left(1-\frac{q^2}{(M_\Delta+M_N)^2}\right)}{\left(1-\frac{q^2}{4{M_N}^2}\right)}\,\frac{G_M^p(q^2)}{\mu_p}\frac{(M_\Delta+M_N)^2}{(M_\Delta+M_N)^2-q^2} \tag{112}$$

where $f_\gamma(0) = 0.122$. It is the $\gamma N\Delta$ coupling constant for real photons.

With respect to the $\vec{S}$ and $\vec{T}$ operators (transition operator between $\frac{3}{2}$ spin states to $\frac{1}{2}$ spin states and respectively between $\frac{3}{2}$ isospin states to $\frac{1}{2}$ isospin states), their normalization is:

$$< \frac{3}{2}, M|S_\lambda^\dagger|\frac{1}{2}, m >= (1\frac{1}{2}\frac{3}{2}|\lambda m M) \tag{113}$$

$$< \frac{3}{2}, M|T_\lambda^\dagger|\frac{1}{2}, m >= (1\frac{1}{2}\frac{3}{2}|\lambda m M) \tag{114}$$

where λ is a spherical basis index.

References

[1] Z.E. Meziani et al. , Phys. Rev. Lett. 52 (1984) 2130; ibid 54(1985)1233

[2] R. Altemus et al., Phys. Rev. Lett. 44 (1980) 965

[3] P. Barreau et al., Nucl. Phys. A402 (1983) 515

[4] G. Orlandini and M. Traini, Rep. Prog. Phys.54 (1991) 257

[5] C. C. Blatchley et al. , Phys Rev. C34 (1986) 1243

[6] T. C. Yates et al. , Phys. Lett. B312 (1993) 382

[7] J. Jourdan, Phys. Lett. B353 (1995) 189; J. Jourdan, Nucl. Phys. A603 (1996) 117

[8] D. Wilkinson, talk at the PANIC 96 conference, Williamsburg, June 1996, C.E. Carlson and J.J. Domingo Edts., World Scientific, pag. 217

[9] J. Noble et al., Phys. Rev. Lett. 46(1981) 412

[10] C. M. Shakin, Nucl. Phys. A446 (1985) 323

[11] M. Bergmann, K. Goeke and S. Krewald, Phys. Lett. B243 (1990) 185

[12] J. D. Walecka, Ann. of Phys. 83 (1974) 491 B.D. Serot and J. D. Walecka, Adv. in Nucl. Phys. 16, ed. J.W. Negele and E. Vogt (plenum, N.J. 1986)

[13] C. J. Horowitz and J. Piekarewicz, Nucl. Phys. A511 (1990) 461

[14] R. J. Furnstahl and C. E. Price, Phys. Rev.C40 (1989) 1398

[15] A. Gil, M. Kleinmann, H. Müther and E. Oset, Nucl. Phys. A584 (1995) 621

[16] M. Kirschbach, D.O. Riska and K.Tsushima, Nucl. Phys. A542 (1992) 616

[17] E.D. Izquierdo, G. Barenboim and A.O. Gattone , Nucl. Phys. A609 (1996) 437

[18] C. J. Horowitz, Phys. Lett. B208 (1988) 8; Ibid, Phys. Rev. Lett. 62 (1989) 391

[19] H. Kurasawa and J. Suzuki, Nucl.Phys. A 490 (1988) 571

[20] C. Mahaux, P.F. Bortignon, R.A. Broglia and C.H. Dasso, Phys. Reports 120 (1985) 1

[21] E. Oset and A. Palanques, Nucl. Phys A 359 (1981) 289

[22] J. Carlson and R. Schiavilla, Phys. Rev. C491 (1994) 2880

[23] W. M. Alberico, T.W. Donnelly and A. Molinari, Nucl. Phys. A 512 (1990) 541

[24] W. M. Alberico, M. Ericson and A.Molinari, Ann. of Phys. 154 (1984) 356

[25] J. W. Van Orden and T.W. Donnelly, Ann. of Phys 131 (1981) 451

[26] M. Kohno and N. Ohtsuka, Phys. Lett. B98 (1981) 335

[27] W. M. Alberico, R. Cenni, A. Molinari and P. Saracco, Phys Rev. Lett. 65 (1990) 1845

[28] J. E. Amaro, G. Co', E. M. V. Fasanelli and A. M. Lallena, Phys. Lett. B 277 (1992) 249

[29] J. E. Amaro, G. Co' and A. M. Lallena, Ann. of Phys. 221 (1993)306

[30] J. E. Amaro, A.M. Lallena and G. Co', Nucl. Phys. A578 (1994) 365

[31] K. Takayanagi, Phys. Lett. B233 (1989) 271,ibid, Phys. Lett. B230 (1989) 12; ibid, Nucl. Phys. A 516 (1990) 276

[32] R. C. Carrasco and E. Oset, Nucl. Phys. A536 (1992) 445

[33] G.E. Cross et.al., Nucl. Phys. A593 (1995) 463

[34] P.D. Harty et.al., Phys. Lett. B380 (1996) 247

[35] T. Helh, Prog. Part. Nucl. Phys. 34 (1995) 385

[36] M. Cavinato, D. Drechsel, E. Fein, M. Marangoni and A.M. Saruis, Nucl. Phys. A423 (1989)376

[37] S. Drozdz, G. Co', J. Wambach and J. Speth, Phys. Lett. B 185 (1987) 287

[38] W. M. Alberico, M. Ericson, A. Molinari and Zi Xing Wang, Phys. Lett. B233 (1989) 37

[39] C. R. Chinn, A. Picklesimer and J. W. Van Orden, Phys.Rev. C40 (1989) 790

[40] Y. Horikawa, F. Lenz and N. Mukhopadhyay, Phys. Rev. C 22 (1980) 1680

[41] A. Fabrocini and S. Fantoni, Nucl. Phys. A 503 (1989)375

[42] P. Fernández de Córdoba and E. Oset, Phys. Rev. C 46 (1992) 1697

[43] A. Ramos, A. Polls, and W, H. Dickhoff, Nucl. Phys. A503 (1989) 1

[44] H. Müther, G. Knehr and A. Polls, Phys. Rev. C52 (1995) 2955

[45] C. Ciofi degli Atti, S. Liuti and S. Simula, Phys. Rev. C41 (1990) 2474

[46] M. J. Dekker et al., Phys. Lett. B 266 (1991) 249

[47] M. Anghinolfi et al., Nucl. Phys. A602 (1996) 405

[48] S. Nozawa and J. S. H. Lee, Nucl. Phys. A513 (1990) 511

[49] E. Oset, H. Toki and W. Weise, Phys. Reports 83 (1982) 281

[50] Y. Horikawa, M. Thies and F. Lenz, Nucl. Phys. A 345 (1980) 386

[51] E. Oset and L.L. Salcedo, Nucl. Phys. A 468 (1987) 631

[52] C. Garcia Recio, E.Oset, L.L. Salcedo, D. Strottman and M.J. Lopez, Nucl. Phys. A 526 (1991) 685

[53] L. L. Salcedo, E. Oset, M.J. Vicente Vacas and C. Garcia Recio Nucl. Phys. A 484 (1988) 557

[54] P. Fernández de Córdoba, E. Marco, H. Müther, E. Oset and A. Faessler, Nucl. Phys. A611 (1996) 514

[55] J. E. Amaro, A. M. Lallena and G.Co', Int. Jour. Mod. Phys. E, 3 (1994) 735

[56] W. M. Alberico, A. Drago and C. Villavecchia, Nucl. Phys A 505 (1989) 309

[57] A. Gil, J. Nieves and E. Oset, University of Valencia preprint, FTUV/97-40

[58] A. Gil, PhD Thesis, University of Valencia, December 1996.

[59] M. G. Olsson, Nucl. Phys. B78 (1974) 55

[60] E. Amaldi, S. Fubini and G. Furlan, *Pion electroproduction*, Springer Tracts in Modern Physics, Vol. 83 (Springer, Berlin, 1979)

[61] K. Baetzner et al., Phys. Lett. B39 (1972) 575

[62] H. Breuker et al., Nucl. Phys. B146 (1978) 285

[63] C. Mistretta et al., Phys. Rev. Vol.184 (1969) 5

[64] L. Ghedira, PhD Thesis, University of Orsay (1986)

[65] E. Oset and W. Weise, Nucl. Phys. A319 (1979) 477

[66] L.L. Salcedo et al., Phys. Lett. B208 (1988) 339

[67] A.L. Fetter and J.D. Walecka, *Quantum Theory of many-particle systems*, McGraw-Hill, 1971

[68] J. Speth et al., Nucl. Phys. A343 (1980) 382

[69] R.C. Carrasco, E. Oset and L.L. Salcedo, Nucl. Phys. A 541 (1992) 585

[70] A. Dellafiore et al., Phys. Rev C 31 (1985) 1088

[71] P. J. Mulders, Phys. Reports 185 (1990) 83

[72] A. Gil and E. Oset, Nucl. Phys. A 580 (1994) 517

[73] A. Zghiche et al. Nucl. Phys. A 572 (1994) 513

[74] A. Braghieri et al., Phys. Lett. B363 (1995) 46

[75] A. Ströher et al., Workshop on N^* resonances, INT, Seattle,

[76] J.A. Gómez-Tejedor and E. Oset, Nucl. Phys. A571 (1994) 667

[77] J.A. Gómez-Tejedor and E. Oset, Nucl. Phys. A600 (1996) 413.

[78] V. Bernard et al., Nucl. Phys. A580 (1994) 475.

[79] M. Benmerrouche and E. Tomusiak, Phys. Rev. Lett. 73 (1994) 400.

[80] J. Heisenberg, Adv. Nucl. Phys. 12 (1981) 61; J. Heisenberg and H.P. Blok, Annu. Rev. Nucl. Part. Sci. 33 (1983) 569.

[81] J.L. Friar and S. Fallieros, Phys. Lett. B 114 (1982) 403; Phys. Rev. C 29 (1984) 1645.

[82] J.E. Amaro, B. Ameziane and A.M. Lallena, Phys. Rev. C53 (1996) 1430.

[83] T. Muta, Foundations of Quantum Chromodynamics, World Scientific 1987.

[84] E. Oset and A. Ramos, Phys. Rev. C53 (1996) 305